SynGAP Controls Synapse Formation by Regulating Spine Development and Morphology

Thesis by

Luis E. Vázquez

In Partial Fulfillment of the Requirements

for the Degree of

Doctor of Philosophy

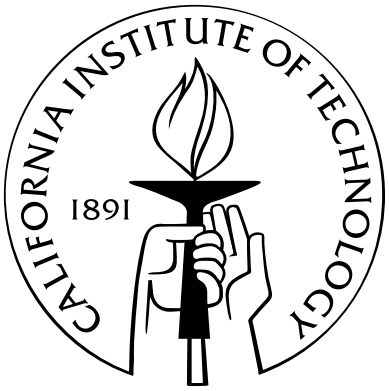

California Institute of Technology

Pasadena, California, 91125

2004

(Defended May 21, 2004)

En agradecimiento de sus esfuerzos por mi familia, dedico todos mis esfuerzos académicos a mi padre, que en paz descansa. No obstante, también dedico esta tesis doctoral- la cúspide de mis estudios- a mi madre, por su amor y apoyo incondicional.

Acknowledgements

First, I am extremely grateful to Mary B. Kennedy for her guidance and support. Many thanks for bringing me to Caltech, believing in me and allowing me to work in your lab, providing equipment and reagents, teaching me numerous techniques, provoking critical thinking, and pushing forward my ability to design experiments. I also appreciate your help in writing the research article. Working in the Kennedy lab was an honor, and I will always remember you dearly.

I am also grateful to the members of my thesis committee, including Scott E. Fraser, Henry Lester, Kai Zinn and Mary B. Kennedy, for valuable input in writing the thesis and doing research.

I would also like to thank the following people for their substantial contribution to my research: Hong-Jung Chen for generating the synGAP *knockout* mouse; Irene Knuesel for the pictures of postnatal day 1 (P1) *knockout* mice, P1-brain immunostaining experiments and numerous constructive discussions; Irina Sokolova and Henry Lester for the electrophysiology; Jeong Oh for creating the GAP domain point mutations; Alan Rosenstein and Shannon O'Dell for mouse genotyping; and Gentry Patrick, Erin Schuman, Peter Seeburg, Julius Zhu and Roberto Malinow for plasmids, Sindbis viruses and reagents. I am also grateful to Gilberto Hernández, Adeline Seah, Margaret Hainline and Lori Washburn for their help with image analysis, and Carene Oliveras for work on the developmental expression of synaptic proteins.

I would particularly like to thank Edoardo Marcora for all the help with the LaTeXtypesetting system, technical support, revisions of this work and constructive discussions; and Pasquale Manzerra and Holly Carlisle for technical support, revisions of this work and constructive discussions.

I would like to thank several people who were instrumental in my scientific development: Leslie Schenker for teaching of hippocampal dissections, neuronal culture and immunostaining; and Wandong Zhang and Shaojun Tang for Molecular Biology training. I am also grateful to Jose Lebrón who recruited me to come to Caltech for graduate school.

I would like to thank those involved in maintaining the synGAP mouse colony: Eugenia Khorosheva for keeping track of the mice, genotyping and organizing the colony; and Vanessa Vargas, Lilia Añonuevo and Jenny Arvizu (Caltech Animal Facility) for arranging the breeding of mice.

I would also like to thank Scott Fraser and the BIC for providing confocal microscopes and microscopy training; Tim Masloski (Zeiss) for help with KS 300 software; and Baris Bingol and Bryan Smith for help with Image J software.

I would like to thank the following for financial support: Joanne Berger-Sweeney and MNFP; Mary Kennedy; Elizabeth Ayala; and Natalie Gilmore and the Caltech Grad Office. I would like to thank Cheryl Gause for placing of orders, scheduling meetings and arranging different events. Also, I appreciate the support from current and former members of the Kennedy lab, and Bonefacio Mazas for lab maintenance.

Finally, I am dearly grateful to Wendy P. Santaella Von Borstel for her love, patience and support. I would have never made it this far without you.

Abstract

SynGAP is a brain-specific Ras GTPase-activating protein that is an abundant component of the signaling complex associated with the NMDA-type glutamate receptor. We generated mutant mice lacking synGAP to study its physiological role. Homozygous mutant mice die in the first few days after birth; however, neurons from mutant embryos can be maintained in culture. Here we report that spine maturation and synapse formation are accelerated in cultured mutant neurons, and the spines of mature mutant neurons are significantly larger than those of *wild type*. Clusters of PSD-95, and subunits of AMPA-type and NMDA-type glutamate receptors are larger and brighter, and appear in spines of mutant neurons by day 10 *in vitro*; whereas in *wild-type* neurons they are still mostly located in dendritic shafts. The frequency and amplitude of miniature excitatory postsynaptic currents are larger in mutant neurons at day 10 *in vitro*, confirming that they have more functional synapses, with more AMPA receptors in them. At day 21 *in vitro*, the spines of mutant neurons remain significantly larger than those of *wild type*. The mutant phenotype at day 10 *in vitro* can be rescued by introduction of recombinant *wild-type* synGAP on day 9. In contrast, introduction of synGAP with a mutated GAP domain or a deletion of the terminal domain that binds to PSD-95 does not rescue the mutant phenotype, indicating that both domains play a role in control of spine maturation. Thus, the GAP activity of synGAP, as well as its association with PSD-95, is important for normal regulation of spine and synapse maturation in hippocampal neurons.

Contents

Chapter 1

Introduction

The dendritic arbor of pyramidal neurons is highly heterogeneous, containing up to thousands of synapses [Schuman, 1999]. Not only postsynaptic density (PSD) architecture, receptor composition, and response to stimulus vary from synapse to synapse, but also they are confined within spines, specialized structures that also vary in size, shape, and density. The ability of spines to change in shape or number (structural plasticity) has been proposed to underlie long-term information storage [Bailey and Kandel, 1993]. The regulation of structural plasticity is critical for physiological wiring of neural circuits [Trachtenberg et al., 2002] during development, learning and memory in adults [Grutzendler et al., 2002], and pathological degeneration during disease [Fiala et al., 2002]. A wealth of knowledge has been gained on the regulation of structural plasticity, and many proteins have been implicated in this process. The identification of proteins shed only some light into this complex process, and further studies are needed to understand their exact role in regulating structural changes of spines [Sanes and Lichtman, 1999]. Here, we show that synGAP controls synapse formation by regulating spine development and morphology. We propose that synGAP mediates these effects by regulating the activity of Ras.

1.1 Historical background on dendritic spines

Dendritic spines were first described more than one hundred years ago by Santiago Ramón y Cajal [Ramon y Cajal, 1888, 1891, Ramon y Cajal] (reviewed in Bon-

hoeffer and Yuste [2002]). Using a silver impregnation method (based on Golgi's original staining technique) Cajal noticed spiny or thorny-like structures (now known as spines) on the dendrites of cerebellar and neocortical cells:

> ...Also, the surface of the Purkinje cells dendrites appear bristling with thorns or short spines, which in the terminal branches are represented by light asperities. Early on we thought that these eminences were the result of a tumultuous precipitation of the silver; but the constancy of their existence and its presence even in preparations where the reaction appears with great delicacy in the remaining elements, incline us to consider them as a normal disposition.

Cajal thought that spines were specialized compartments of the dendrite that receive information from axons [Ramon y Cajal, 1891]. This was confirmed much later with the advent of electron microscopy, which provided unprecedented detail of the ultrastructure of spines [Gray, 1959, Peters and Kaiserman-Abramof, 1970]. By late 1970s, spines were thought to be stable postsynaptic structures basically consisting of a thin neck and a wider head, although their exact morphology widely varied (Fig. 1.1A). A closer look at spines also revealed a dense thickening of the postsynaptic membrane, thus named the postsynaptic density, or PSD [Cohen et al., 1977] (Section 1.5).

Around the same time, development of biochemical fractionation methods allowed for the purification of synaptic membranes (synaptosomes) and PSDs [Banker et al., 1974, Cotman et al., 1974]. Further studies led to detection of the structural element actin, and the signal-transduction protein calmodulin in the PSD [Blomberg et al., 1977]. Soon afterward, Kennedy and coworkers identified Ca^{2+} /calmodulin-dependent protein kinase II (CaMKII) as a major component of the PSD [Kennedy et al., 1983]. This finding sparked the notion that the PSD serves as a signal-transduction system beneath the postsynaptic membrane (reviewed in Kennedy [1997]). Indeed, over the past twenty years, receptors, scaffolds, cytoskeleton-anchoring proteins and kinases, among other signal-transduction proteins, have been identified in

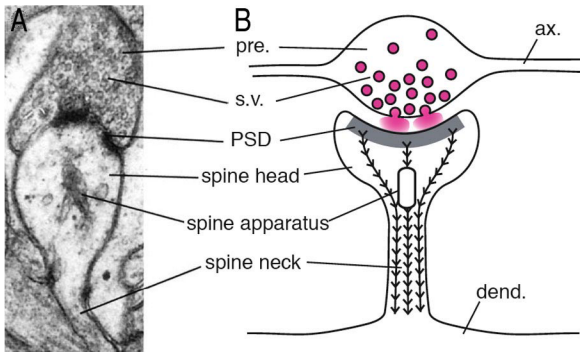

Figure 1.1: **Ultrastructure of a spine.** (A) A single spine synapse seen by electron microscopy. (B) A diagram of a spine structure. The neurotransmitter glutamate (pink) is stored within synaptic vesicles and released into the synaptic cleft where it activates receptors located in the postsynaptic density (PSD). Actin filaments are represented by the barbed lines. ax., axon; pre., presynaptic bouton; dend., shaft of dendrite; s.v., synaptic vesicle. Adapted from Matus [2000].

the PSD (reviewed in Kennedy [2000], Sheng and Sala [2001]).

Currently, many studies are aimed at understanding the regulation of spine morphology, the dynamic aspect of spine development, and the signaling cascades underlying synaptic plasticity. These topics will be further reviewed here.

1.2 Spine morphology

There is a wide diversity in the morphology of spines. This is evident even within a few microns of dendrite (Fig. 1.2A). Stereotypically, spines consist of a thin neck and a head. However, some spines lack a neck (stubby spines) while others lack a head (filopodia). In pyramidal neurons of the hippocampus, spine length ranges from $\sim$0.2 to 6 µm and their width ranges from $\sim$0.1 to 1 µm in diameter [Sorra and Harris, 2000]. Moreover, spine morphology is modulated by a wide variety of environmental factors, including synaptic activity [Maletic-Savatic et al., 1999, Engert and Bonhoeffer, 1999, Wu et al., 2001], growth factors [McAllister et al., 1996, Alonso et al., 2004], hormones [Woolley and McEwen, 1994] and possibly spatial constrictions of the neuropil [Edwards, 1998].

Despite their wide range of morphologies, protrusions can be classified as filopodia or spines, which can be further classified as stubby-, thin-, or mushroom-shaped based

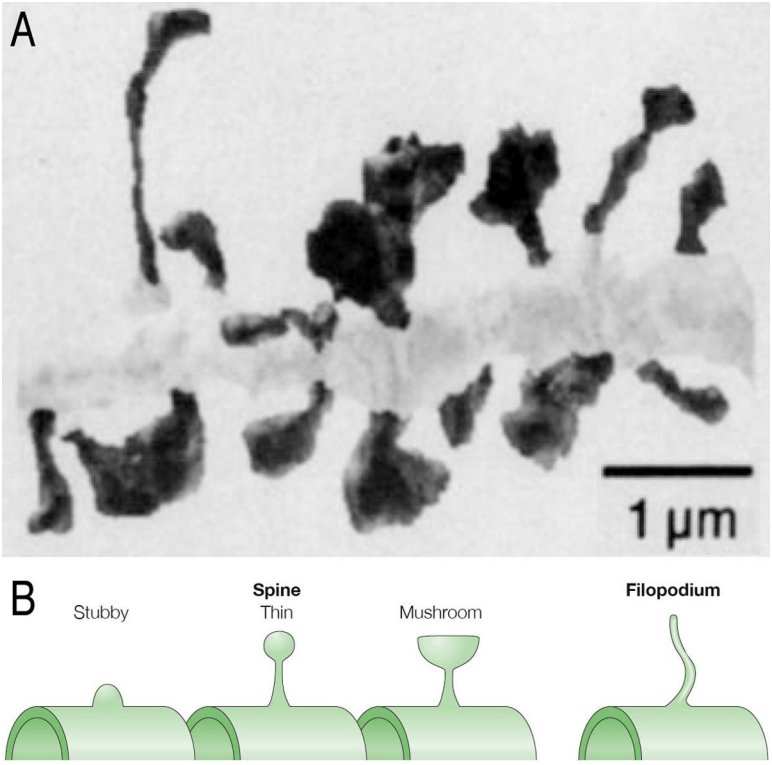

Figure 1.2: **Spine morphology.** (A) Electron microscopy (EM) reconstruction of a dendritic segment depicting the wide diversity in spine morphology. Adapted from from Harris and Kater [1994]. (B) Schematic drawing of spine morphologies, categorized as described in Peters and Kaiserman-Abramof [1970]. Adapted from Yuste and Bonhoeffer [2004].

on their appearance (Fig. 1.2B). In general, filopodia are long and thin, lack a PSD, and are highly motile. In addition, filopodia prevail early in development, and are thought to be precursors of spines [Fiala et al., 1998]. Spines, in the other hand, have a PSD, are less dynamic, and prevail over filopodia in the adult brain [Grutzendler et al., 2002, Trachtenberg et al., 2002]. Also, they are generally accompanied by an active presynaptic bouton and are capable of synaptic transmission, and the strength of synaptic transmission is presumably correlated with the size of spines [Bailey and Kandel, 1993, Yuste and Bonhoeffer, 2001, Harris et al., 2003].

1.3 Spine and synapse formation

It is important to note that there are differences between spine formation (spinogenesis) and synapse formation (synaptogenesis) in the hippocampus. Spine formation refers to the process in which protrusions elongate from the dendritic shaft to sense the environment; it does not imply the formation of a new synapse. It can occur within a few minutes, and in the absence of a presynaptic counterpart. Synapse formation is a much longer and complex process, taking days or even weeks to complete, that involves the encounter and adhesion of pre- and post-synaptic terminals. From a strictly postsynaptic perspective, this process generally begins with spine formation, followed by shortening of length, widening of the spine head and decrease in motility [Sorra and Harris, 2000]. These morphological changes that spines undergo during synapse formation are referred to as spine maturation. Notwithstanding their differences, synapse formation and spine maturation are closely related and the terms will here be used interchangeably.

There are three proposed models of synapse formation: the Sotelo, Miller/Peters and filopodial models (reviewed in Yuste and Bonhoeffer [2004]). In the Sotelo model, spines emerge independently of the axon terminal whereas in the Miller/Peters model, the terminal actually induces the formation of the synapse. In the filopodial model, a dendritic filopodium captures an axonal terminal and becomes a synapse (Fig. 1.3). Spine formation in 'Sotelo-fashion' is particularly exhibited by spines on Purkinje cells

of the cerebellum whereas the Miller/Peters and filopodial models are both evident in pyramidal neurons of the neocortex. Nevertheless, there is increasing evidence that the filopodial model prevails in the hippocampus [Sorra and Harris, 2000, Matus, 2001, Yuste and Bonhoeffer, 2004].

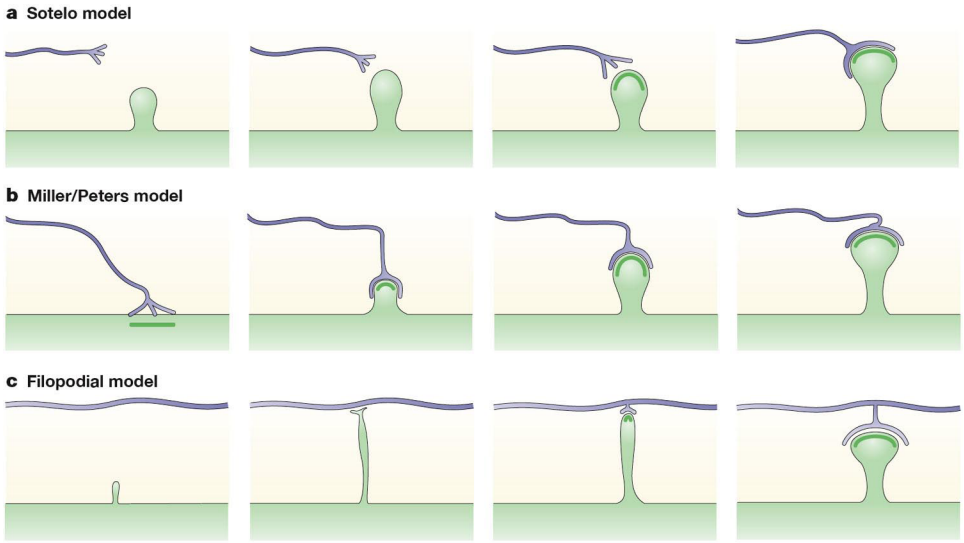

Figure 1.3: **Three models for spine formation.** In the Sotelo model (a), spines emerge independently of the axon terminal. In the Miller/Peters model (b), the terminal actually induces the formation of the spine. Finally, in the filopodial model (c), a dendritic filopodium captures an axonal terminal and becomes a spine. Adapted from Yuste and Bonhoeffer [2004].

Recent studies provided further support to the filopodial model of spine maturation through time-lapse imaging of the process [Okabe et al., 2001, Marrs et al., 2001]. In addition to visualizing the morphological changes characteristic of filopodial-type maturation, they also visualized incorporation of PSD-95, as a marker of the PSD, in spines. An interesting observation from these studies was that spines that were stable for hours (with only minor morphological changes) contained PSD-95, whereas those that turned over in minutes lacked PSD-95 (reviewed in Matus [2001]). These observations led to a more complete picture of the process of spine maturation, from formation of a filopodia that develop into protospines (spines lacking a PSD) and finally mature into relatively stable spines (Fig. 1.4).

Filopodia, protospines and spines coexist in dendrites of developing neurons, and can be identified in snapshots of dendrites and PSD-95 clusters from neurons in their

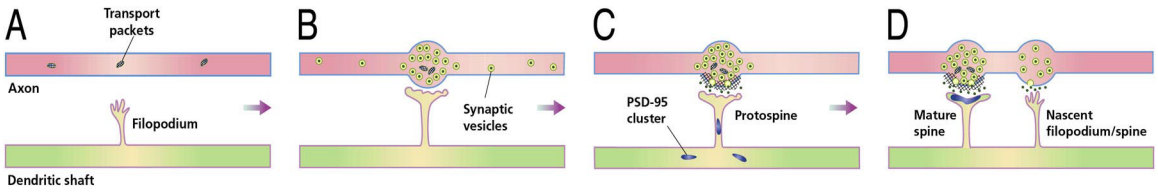

Figure 1.4: **Scheme of synapse formation.** (a) Before making contact with axons, dendrites send out numerous transient filopodia that extend and contract, rapidly 'feeling out' the space around them; at this stage, axons contain widely distributed polymorphic 'transport packets'. (b) Shortly after a dendritic filopodium contacts an axon, vesicles accumulate in varicosities at the same site, suggesting that the dendritic component sends a vesicle recruitment signal to the axon. (c) Some of these vesicles are 'transport packets' containing components of the presynaptic junctional complex (indicated by cross-hatching), which become inserted into the surface membrane at the site of contact. Others are synaptic vesicles, which begin releasing neurotransmitter (indicated by black spots) and thus initiate synaptic signaling. (d) The presence of an active presynaptic terminal induces the recruitment of PSD-95-containing clusters to postsynaptic junctional sites in the heads of developing spines to form a mature spine synapse. Neurotransmitter release from axon terminals may induce the outgrowth of new filopodia and spines. Adapted from Matus [2001].

tenth day of growth in culture (Fig. 1.5). From such images, we can measure spine density, length and head-width of spines, and percent of spines containing PSD-95, which provide a semi-quantitative measure of spine maturity. It also allows us determine the influence of a variable on spine maturation by determining whether the filopodia-spine equilibrium is shifted towards less or more mature. This is in fact, the basis of our study (Chapter 3).

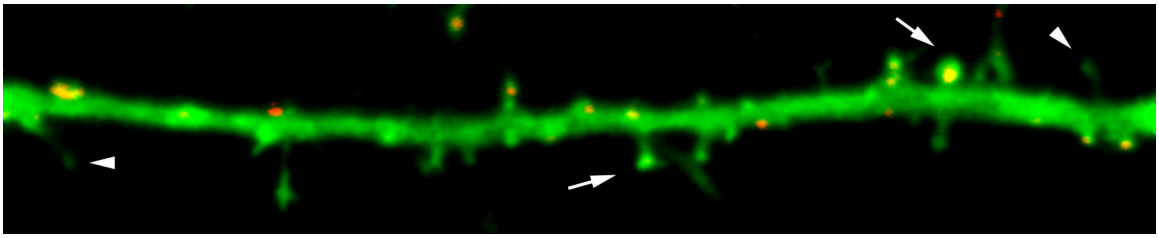

Figure 1.5: **Snapshot of spine maturation.** Dendrite of a 10 DIV GFP-expressing neurons (green) stained for PSD-95 (red). Filopodia (*arrowheads*), spines without PSD-95, or protospines (*bottom arrow*), and mature spines bearing PSD-95 (*top arrow*) can be identified at this developmental age.

1.3.1 Spine formation in the adult brain

Synapse formation begins during the first week of postnatal development and persists throughout adulthood, although at slower rates [Grutzendler et al., 2002, Trachtenberg et al., 2002]. Thus, regulation of spine formation and maturation is relevant not only during development, but also in the adult brain. This raises the question, what is the role of synapse formation in the adult brain?

It is thought that formation and retraction of spines in the adult brain underlies learning and memory [Ramon y Cajal, Bailey and Kandel, 1993, Smart and Halpain, 2000, Zito and Svoboda, 2002]. Supporting this idea, it has been shown *in vitro* that strong stimuli that lead to long-term enhancement of synaptic efficacy (LTP), can induce formation of new spines in the potentiated region of a dendrite [Maletic-Savatic et al., 1999, Engert and Bonhoeffer, 1999]. The authors concluded that the activity-induced structural changes contribute to the development and refinement of neural circuitry. Also, two recent studies showed that sensory stimulation induces spine formation in the cortex of freely moving rodents (reviewed in Zito and Svoboda [2002]). One study used time-lapse microscopy to show that sensory deprivation reduced protrusive motility of filopodia in deprived regions of the barrel cortex during development (P11- P13) [Lendvai et al., 2000]. The other study used electron microscopy to show that in adult mice, single whisker stimulation increased the total synaptic density in the corresponding cortical barrel [Knott et al., 2002]. These studies also showed that although the changes in spine structure were transient, they led to alterations in synaptic circuitry even in adulthood.

1.3.2 'Silent synapses'

Another criterion by which a spine is thought to mature, aside from morphology, is the recruitment of AMPA-type glutamate receptors (AMPAR) to the postsynaptic membrane (reviewed in [Malinow and Malenka, 2002]). Early in neuronal development, many synapses contain NMDA-type glutamate receptors (NMDAR) and lack AMPARs [Petralia et al., 1999, Liao et al., 1999]. The NMDAR-only containing

synapses are referred to as 'silent synapses' because under basal conditions they do not depolarize in response to glutamate. Later in development (corresponding to the second week of neuronal growth in culture), increased expression and synaptic delivery of AMPARs 'un-silences' the previously 'silent' synapses (reviewed in Scannevin and Huganir [2000], Sheng and Lee [2001], Malinow and Malenka [2002]). Thus, spines containing both NMDA- and AMPA-receptors are considered functioning mature spines.

Recruitment of AMPARs to the postsynaptic membrane is also triggered by LTP-inducing stimuli, and depends on NMDAR activation [Isaac et al., 1995, Liao et al., 1995, Durand et al., 1996, Heynen et al., 2000]. Therefore, one mechanism by which a synapse might be strengthened is by rapid insertion of AMPARs (the 'silent synapse hypothesis'). This hypothesis provoked an interest in AMPAR trafficking and has produced a large body of data on the regulation of receptor expression at excitatory synapses [Shi et al., 1999, Lin et al., 2000, Ehlers, 2000, Shi et al., 2001, Passafaro et al., 2001]. One recent study described signal-transduction events initiated by the NMDAR that lead to synaptic insertion of AMPARs [Zhu et al., 2002]. The authors show that influx of Ca^{2+} through the NMDAR initiates a signaling cascade involving CaMKII, the small GTPase Ras, and the p42/44MAPK (or ERK; extracellularly regulated kinase) cascade. This cascade results in rapid insertion of intracellular AMPARs in the synapse (Fig. 1.6). Consistent with this, Zhu also noticed that chronic blockade of the NMDAR during a critical period of development leads to a decrease in AMPAR-to-NMDAR current ratio [Zhu and Malinow, 2002]. Given the results presented in Chapter 3, it will be interesting to determine whether synGAP, a downregulator of Ras activity, has a role in Ras-mediated AMPAR trafficking.

1.4 The actin cytoskeleton of dendritic spines

Dendritic spines are rich with actin filaments in contrast to the dendritic shaft, where the microtubule cytoskeleton predominates [Matus et al., 1982, Fifkova and Delay, 1982, Fischer et al., 1998]. The dynamic nature of actin polymerization has an essen-

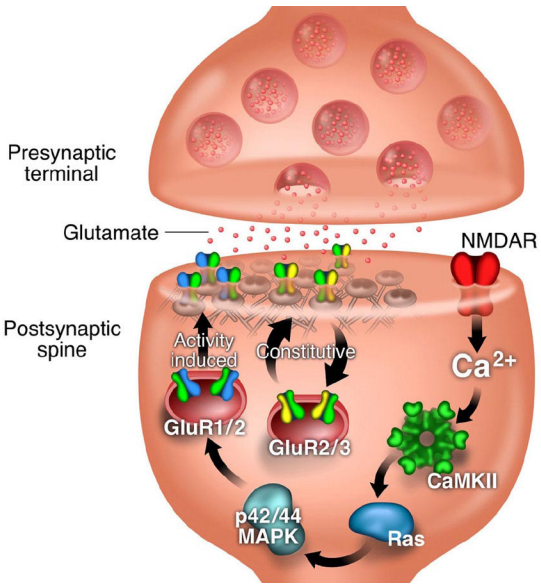

Figure 1.6: **Insertion of AMPA receptors into the synapse.** Cartoon representation of pathways thought to be involved in the regulated insertion of AMPA receptors into the synapse. Influx of Ca2+ into the postsynaptic spine through NMDA receptors (NMDAR) initiates a signaling cascade involving CaMKII, the small GTPase Ras, and the p42/44 MAPK cascade. This cascade results in the rapid insertion of intracellular GluR1-containing AMPA receptors into the synapse and thus an increase in postsynaptic responsiveness. GluR2-GluR3 AMPA receptors do not undergo activity-induced insertion, but instead are involved in constitutive recycling into the membrane. AMPA receptors are maintained at the synapse by physical interaction with scaffolding proteins present in the postsynaptic density. Adapted from Contractor and Heinemann [2002].

tial role in spine formation and activity-dependent spine motility [Nakayama et al., 2000, Tashiro et al., 2000, Fischer et al., 2000]. This raises the question, what are the biochemical pathways regulating the actin rearrangements in spines?

There is increasing evidence that actin rearrangements are controlled by the Rho family of small GTPases. Rac promotes the development of new spines while Rho blocks their formation and maintenance (reviewed in Nakayama and Luo [2000], Luo [2002], Bonhoeffer and Yuste [2002]. Other components of the Rac pathway have also been implicated in spine formation. Kalirin, a RacGEF, promotes spine formation [Penzes et al., 2001, Ma et al., 2003] whereas absence of LIM Kinase-1 (LIMK-1), a downstream effector of Rac, leads to decreased head width of spines [Meng et al., 2002].

In addition of Rac and Rho, other small GTPases, such as Rnd and Rap, also play roles in actin rearrangements and spine motility [Ishikawa et al., 2003, Pak et al., 2001]; the role of Ras though, is much less clear. One study showed that repeated depolarization stimuli caused a sustained phosphorylation of MAPK (a downstream effector of Ras) and growth of filopodia [Wu et al., 2001]. In this study, we show that absence of synGAP, a down-regulator of Ras, leads to accelerated spine formation (Chapter 3). Although it remains to be tested, it seems that Ras also promotes development of new spines. It will also be interesting to determine whether this occurs via Rac or another pathway; and how the small GTPases work in conjunction, synergize, or antagonize each other for the precise regulation of spine formation.

1.5 The postsynaptic density

At the postsynaptic membrane of pyramidal neuron excitatory synapses, neurotransmitter receptors are associated with a large number of proteins, forming the postsynaptic density (PSD). This large complex of proteins extends approximately 30 nm from the postsynaptic membrane into the cytosol, anchoring to the actin cytoskeleton [Sheng, 2001, Kennedy, 2000]. The PSD can be easily purified by detergent extraction of biochemically isolated synaptic membranes; subsequent detergent washes strip

loosely-bound proteins from the PSD and a core complex of proteins remains, called the PSD fraction (reviewed in Kennedy [1997]). Many of the proteins present in the PSD and the PSD fraction have been identified [Walikonis et al., 2000, Husi et al., 2000], ranging from cell adhesion proteins, receptors, scaffolding proteins and signaling proteins, among others (Fig. 1.7) (also see Kennedy [1998], Sheng and Kim [2000], Xiao et al. [2000]). The presence of vast signal-transduction proteins supported the notion that the PSD functions as a signaling machine that can respond to stimuli, and accordingly regulate the strength of synaptic transmission [Kennedy, 2000, Sheng and Sala, 2001].

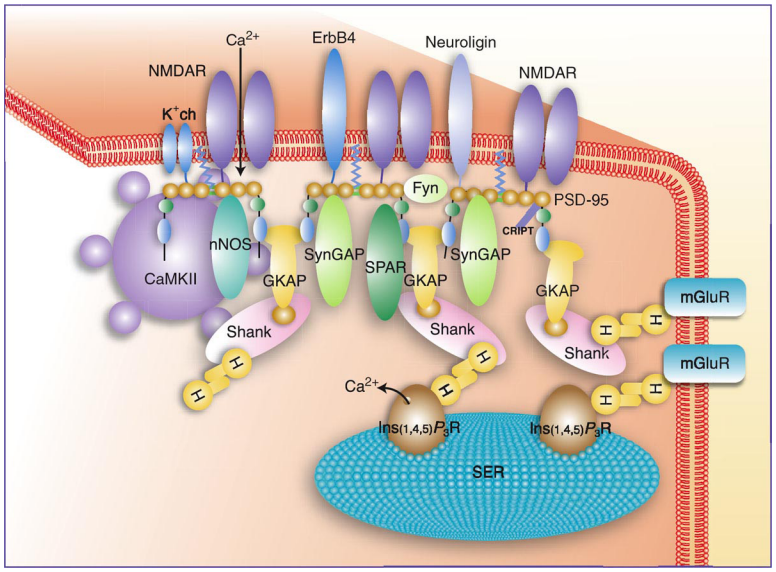

Figure 1.7: **Schematic drawing of the PSD.** NMDARs are anchored in the PSD by interactions between the cytoplasmic C-terminal tails of their NR2 subunits and the PDZ domains (orange) of PSD-95, an abundant PSD protein that forms a two-dimensional lattice immediately under the postsynaptic membrane. Having multiple domains that bind to a variety of cytoplasmic proteins, PSD-95 functions as a scaffold to assemble a specific set of signaling proteins around the NMDAR. These proteins, such as neuronal nitric oxide synthase (nNOS), SynGAP [a GTPase-activating protein (GAP) for Ras] and SPAR (a GAP for Rap), may participate in downstream signaling by NMDARs. PSD-95, in turn, interacts with GKAP and Shank, two scaffold proteins lying in the deep part of the PSD. Shank binds to Homer, which interacts directly with the cytoplasmic tail of the metabotropic glutamate receptor (mGluR). Homer forms multimers and additionally binds to the inositol 1,4,5-trisphosphate receptor [Ins(1,4,5)P3R] found in smooth endoplasmic reticulum (SER), thereby linking cell surface mGluRs to a downstream effector [Ins(1,4,5)P3R] in intracellular calcium stores. Thus an extensive network of protein-protein interactions within the PSD links together different classes of postsynaptic glutamate receptor and couples them to specific intracellular signaling pathways.Adapted from Morgan Sheng.

The tightly bound proteins in the PSD fraction are considered the core of the PSD. Major components of the PSD fraction include the NMDAR, the scaffold PSD-95, and the signal transduction proteins CaMKII and synGAP. Thus, CaMKII and synGAP might be crucial in initiating a variety of biochemical responses triggered by influx of Ca^{2+} through the NMDAR into the spine. NMDAR-mediated biochemical responses underlie synapse formation during development [Constantine-Paton et al., 1990] and synaptic plasticity in the adult brain [Malenka and Nicoll, 1993]. Here, we focus on the role of synGAP on synapse formation.

1.5.1 SynGAP

SynGAP is a brain-specific, 135 KDa Ras GTPase activating protein (GAP) [Chen et al., 1998, Kim et al., 1998]. It contains PH and C2 domains, a GAP domain, a proline-rich region, and a t-T/SXV motif (Fig. 1.8). It is a major component of the PSD at glutamatergic postsynaptic terminals, where it associates with the PDZ domains of PSD-95 via its carboxyl terminal t-T/SXV domain [Chen et al., 1998, Kim et al., 1998, Zhang et al., 1999], competing with a variety of other potential binding partners for PSD-95 [Kennedy, 2000, Sheng and Sala, 2001]. Four splice variants of synGAP, taken together, are approximately as abundant in the PSD fraction as PSD-95 itself [Chen et al., 1998, Li et al., 2001], suggesting that it is an effective competitor *in vivo*. Ca^{2+} /calmodulin-dependent protein kinase II (CaMKII), another abundant protein in the PSD complex, phosphorylates synGAP [Chen et al., 1998] and thereby increases its GAP activity [Oh et al., 2004]. Because CaMKII is activated by Ca^{2+} ions flowing through the NMDA receptor, we hypothesize that synGAP may act as a point of integration between NMDA receptor activation and Ras signaling pathways.

Komiyama et al. [2002] and Kim et al. [2003] generated mice lacking synGAP to study the function of synGAP in neurons. Both groups found that synGAP heterozygotes (*het*) have a specific defect in hippocampal LTP. Komiyama et al. also reported that the levels of basal and NMDAR-induced ERK phosphorylation were elevated in *het* mice, suggesting that synGAP is an *in vivo* down-regulator of the

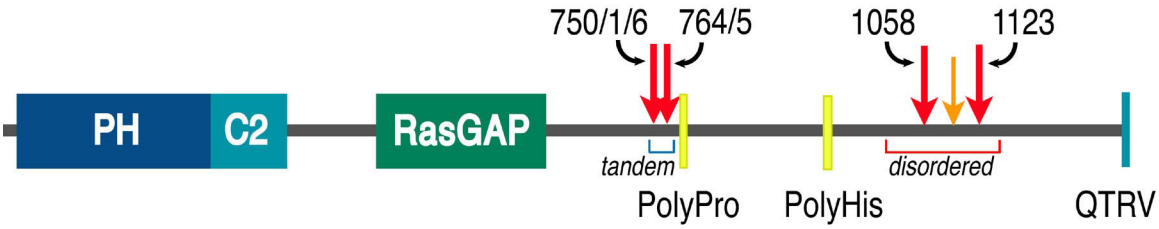

Figure 1.8: **Scheme of synGAP protein.** SynGAP is a 135 KDa protein containing PH and C2 domains, a GAP domain, proline-rich and poly-His regions, and a t-T/SXV motif. It is a major substrate for CaMKII; phosphorylation by CaMKII increases its GAP activity ∼2-fold. Adapted from Oh et al. [2004].

Ras/ERK pathway. In NMDAR-dependent spatial tasks synGAP *het* mice exhibited slightly impaired rates of learning and normal rates of forgetting [Komiyama et al., 2002]. Komiyama et al. concluded that SynGAP contributes to the induction machinery for memory encoding but not to the persistence of memory traces over time. These results set the stage for a detailed characterization of the role of synGAP in cellular/molecular phenomena underlying learning and memory, which are the focus of the work presented here (Chapter 3).

Chapter 2

Materials and Methods

2.1 Gene targeting construct

Hong-Jung Chen created the gene targeting construct in the following manner. Twelve synGAP genomic DNA fragments were isolated by screening a λFIX II mouse genomic library (129 SvJ strain) with a cDNA probe encoding the PH and C2 domains of the synGAP protein. Genomic sequences used to generate the final targeting construct were derived from a single ∼17 Kb genomic segment. The starting targeting vector pPNTloxPv2 (kindly provided by Dr. Jeong Kyo Yoon at Caltech) was a modified version of pPNT [Tybulewicz et al., 1991] in which the Neo cassette is flanked by two loxP sites. The short arm of the synGAP targeting construct was a 2.4 Kb fragment of intron 3 of the synGAP genomic DNA. It was inserted at the 5' end of the Neo cassette upstream of the first loxP site in pPNTloxPv2. The long arm included a 5.6 Kb genomic fragment containing exons 4 to 9 with intervening introns inserted at the 3' end of the Neo cassette downstream of the second loxP site. This sequence was followed by a 136 bp fragment from the vector pRAY2 (gift of P. Seeburg) containing a third loxP site and 1.5 Kb of the synGAP gene including introns 9 through 11 and exons 10 and 11 (Fig. 3.1A).

2.2 Generation of mouse ES cells for injection into blastocysts

Hong-Jung Chen generated synGAP deleted mouse ES cells in the following manner. Twenty micrograms of linearized targeting construct were electroporated into $1x10^7$ cells/ml of mouse ES (CJ7) cells. The transfected ES cells were grown in the presence of G418 (180 µg/ml) and FIAU (0.2 µM) for 9 days to select for homologous recombinants. Twelve recombinant clones were identified and confirmed by genomic Southern blots with probes flanking the targeted genomic sequences. Two of these clones were expanded for generation of synGAP *knockout* and floxed mutant ES cells. They were transfected with the Cre expressing vector pOG231 (kindly provided by Dr. Henry Lester at Caltech) by electroporation. Twenty eight G418 sensitive clones were identified. The genotypes of these clones were determined by PCR analyses. Two of the clones had complete deletion of sequences between exons 4 and 9 of synGAP (*knockout*; *ko*). Two clones with the *ko* genotype both of which had normal karyotypes, were used for injection into blastocysts to generate chimeras. Injections and breeding of chimeras were performed by the Transgenic Mouse Core Facility at Caltech.

The synGAP *ko* mutation described here is maintained in a heterozygote line and has been back-crossed onto a C57/B6 background. Crossing synGAP heterozygous (*het*) mice results in progeny with a Mendelian distribution (1 *wt*: 2.4 het: 1.3 *ko*, n=138).

2.3 Genotyping

Genomic DNA was isolated from mouse tails and used for PCR with a set of three primers; one recognizing a 3' synGAP sequence (MGIN-11; 5'-GAGAGAGATGGAGGGTCACTTGAG-3') and two recognizing 5' sequences, either within synGAP (MGEX9-1; 5'-CGGATGCTATGTGCAGTGCTGGA-3'), or within the LoxP site (Lox-DS; 5'-GAAGAGGAGTTTACGTCCAGCCAAGCT-3'), in *wild type* (*wt*) or

ko, respectively. PCR cycles started with denaturation of DNA at 94 ℃ for 2 min followed by 35 cycles consisting of denaturation (95 ℃, 30 s), annealing (58 ℃, 30 s), and extension (72 ℃, 2 min) followed by a final extension at 72 ℃ for 10 min. The products were a 1.8 Kb fragment from *wt*, and a 1.7 Kb fragment from *ko* (Fig. 3.1B).

2.4 Primary neuronal culture

Hippocampi from individual mice at embryonic day 16 or 17 were dissected, dissociated by trypsin treatment and mechanical trituration, and plated onto polylysine/laminin (Sigma, St. Louis, MO) coated glass coverslips (12 mm in diameter) at a density of ∼400 neurons/mm^2. Cultures were maintained in neurobasal medium (Gibco, Grand Island, NY) complemented with B27, glutamate, and GlutaMAX-1 (Gibco) as described [Brewer et al., 1993]. To confirm that cell density was similar between *wt* and *ko* cultures, cell counts of Hoechst (Molecular Probes, Eugene, OR)-stained nuclei were done on a set of 21 day *in vitro* (DIV) cultures (Fig. 2.1A). The gross morphology of synGAP *ko* neurons in culture was indistinguishable from that of *wt* neurons (Fig. 2.1B).

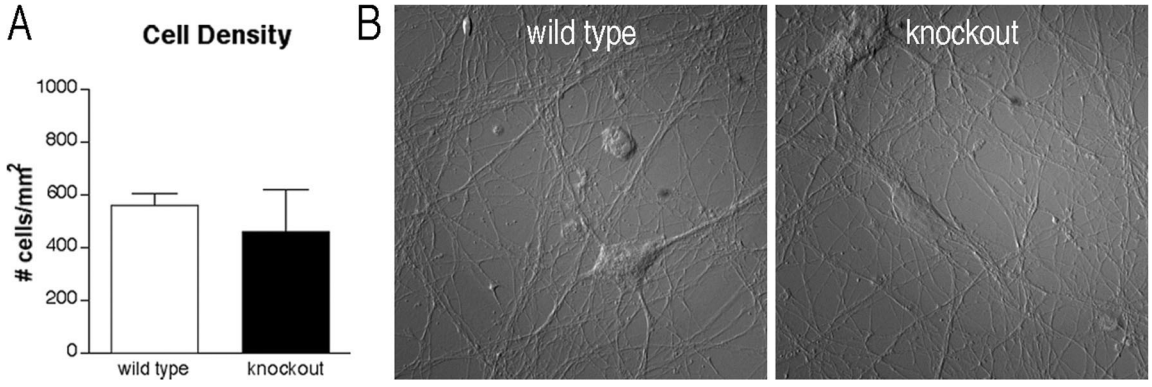

Figure 2.1: **Primary neuronal cultures.** (A) Density of cells in *wt* and *ko* neuronal cultures. Cell density, which includes neurons and glia, in *wt* and *ko* cultures was not significantly different ($P < 0.05$; Student's t-test). (B) Representative high magnification DIC images from *wt* and *ko* neurons. The gross morphology of synGAP *ko* neurons in culture was indistinguishable from that of *wt* neurons.

2.5 Immunocytochemistry

After 10 or 21 DIV, coverslips were rinsed briefly in ice-cold PBS, and fixed with ice-cold 4% paraformaldehyde and 4% sucrose in PBS for 5–10 min. Coverslips were rinsed in ice-cold PBS followed by ice-cold methanol, incubated in methanol at -20 °C for 20 min, washed once with PBS for 15 min, and blocked with 5% NGS, 0.05% Triton X-100 in H-PBS (450 mM NaCl, and 20 mM phosphate buffer, pH 7.4) for at least 1 h at 4 °C. Primary antibodies were added in blocking buffer and cultures on coverslips were incubated ON at 4 °C. The following antibodies and dilutions were used for immunofluorescent staining: rabbit anti-synGAP, mouse anti-PSD-95, mouse anti-NR1 (Affinity BioReagents, Golden, CO; 1:500), rabbit anti-GluR1 (Chemicon, Temecula, CA; 1:100), and rabbit anti-synapsin I (Cho et al. [1992]; 1:1000). After three washes in blocking buffer, coverslips were incubated in goat anti-rabbit or goat anti-mouse secondary antibodies conjugated to Alexa568, or Alexa680 (Molecular Probes, 1:200 each) at room temperature for 1 h. Coverslips were washed once in blocking buffer for 15 min, twice in PBS for 15 min, post-fixed for 5 min with 2% paraformaldehyde in PBS for 5–10 min, washed twice in PBS for 10 min, and mounted on slides with a drop of ProLong® antifade reagent (Molecular Probes).

2.6 Immunoblotting

Cultured hippocampal neurons maintained for 21 DIV were lysed in RIPA lysis buffer (50 mM Tris, pH 8, 2 mM EDTA, pH 8, 150 mM NaCl, 1% Nonidet P-40, 0.5% Deoxycholate, 0.1% SDS, 0.5 mM DTT) containing a cocktail of protease inhibitors (Complete™, Roche, Indianapolis, IN). Protein concentration was determined by the bicinchonic acid (BCA) method (Pierce, Rockford, IL) with bovine serum albumin as a standard. Protein samples (10 µg) were fractionated by SDS-PAGE and electrophoretically transferred to nitrocellulose filters (Schleicher and Schuell, Keene, NH). Filters were blocked for 1 h in TBS, 0.1% Tween-20, 5% nonfat milk at room temperature and incubated with primary anti-synGAP antibodies (Affinity Biore-

agents) at 1:2000 dilution in blocking buffer overnight at 4℃, washed three times in blocking buffer, incubated in goat anti-rabbit IgG conjugated to horseradish peroxidase 1:2000 (Chemicon). Protein bands were visualized by chemiluminescence with SuperSignal® (Pierce), according to manufacturer instructions.

2.7 Viral constructs and infections

Sindbis-eGFP virus was provided by E. Schuman and nsp2S-eGFP (nsp2S is a variant of Sindbis virus) was provided by P. Seeburg. Sindbis viruses expressing eGFP and FLAG-tagged synGAPs were constructed as follows. Sequences encoding eGFP, IRES2 (an internal ribosome entry site), and synGAP were inserted into viruses in tandem to permit independent expression of the two proteins with stronger expression of eGFP than of synGAP. DNA sequence encoding eGFP preceded by a Kozak sequence was obtained from pLP-IRES2-EGFP (BD Biosciences, San Jose, CA) by PCR with high fidelity Taq polymerase (Roche), a 5' oligo containing a ClaI and XbaI linker, and a 3' oligo containing a PstI linker. Similarly, DNA sequence encoding an internal ribosome entry site (IRES2) was obtained from pLP-IRES2-eGFP by PCR with a 5' oligo upstream of a BamHI site in the vector, and a 3' oligo containing a NotI site. This procedure resulted in inclusion of a Kozak sequence at the 3' end of the IRES. For construction of the virus expressing *wild-type* synGAP (synGAP^{wt}), a cDNA encoding flag-synGAP (gift of Dr. Jeong Oh) was amplified by PCR with a 5' oligo containing a NotI site and a 3' oligo containing a SacII site. The eGFP, IRES2, and synGAP segments were subcloned in tandem into the multiple cloning site of pBSK II (-) (eGFP-IRES2-flag-SynGAP). DNA sequencing of this construct revealed no mutations. It was digested with XbaI and SacII, the SacII site was blunted with ExoT (NEB, Beverly, MA), and ligated into the XbaI and StuI sites of pSinRep5 (Invitrogen, Carlsbad, CA) or nsp2S (Fig. 2.2). Viral particles encoding eGFP-IRES2-wtSynGAP were produced according to Invitrogen instructions. Sindbis and nsp2S viral particles gave similar results and were used interchangeably.

The ΔSXV mutant was created by amplifying the flag-synGAP cDNA with a 5'-

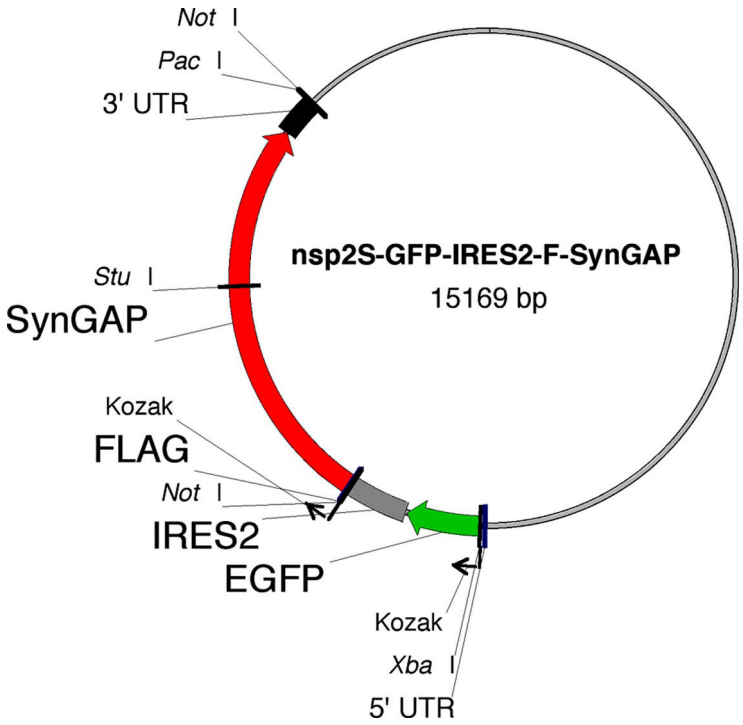

Figure 2.2: **Nsp2S-eGFP-IRES2-SynGAP vector.**

oligo containing a NotI site and a 3'-oligo designed to substitute a stop codon followed by a SacII site for the terminal 5 amino acids (QQTRV) and incorporated into nsp2S as described above.

To construct a virus expressing synGAP with an inactive GAP domain, three point mutations were created in the flag-synGAP sequence by site-directed mutagenesis; R470A, L580I, R581E. Mutations homologous to these three mutations reduce the catalytic activity of the GAP domain of p120 RasGAP several fold [Ahmadian et al., 1997, Skinner et al., 1991]. Mutagenic oligonucleotides (18-25 mers) that contained codons for the indicated mutations were synthesized at the Caltech Oligonucleotide Synthesis Laboratory. The oligonucleotides were phosphorylated at the 5' end by T4 kinase, then annealed to the denatured synGAP plasmid (pSinRep5) at room temperature for 30 minutes. The oligonucleotides were extended with T4 DNA polymerase and T4 DNA ligase *in vitro* to generate a hemi-methylated, double-stranded DNA molecule. A restriction digestion was performed with Dpn-1 to eliminate non-mutant plasmid DNA (those with two methylated strands). The DNA molecules were then

transformed into the E. *coli* mutS strain (deficient in the methylation-specific repair system) and colonies were screened by DNA sequencing for plasmids containing the desired mutations [Kramer et al., 1984]. Viral particles were produced as described above.

Neurons were infected by adding the viruses ($\sim$0.5 µl) to the culture medium on the 9^{th} or 20^{th} DIV. The neurons were incubated in normal growing conditions for 16–20 h following infection, then fixed as described above.

2.8 Light, epifluorescence and confocal microscopy

A Zeiss Axiovert 200 Microscope was used for epifluorescence and light microscopy (Fig. 2.3). Images were acquired with a Plan-Apochromat 63x/1.4 oil objective and a high-resolution CCD camera (Axiocam MRm) under the control of a computer equipped with AxioVision 3.1 (Zeiss). Exposure times were set so that pixel brightness was not saturated, and were held constant during acquisition of all images (1300 x 1030 pixels) for each experiment. For some experiments a Zeiss 510 laser-scanning microscope (LSM) was used for confocal fluorescence microscopy. The pinhole aperture of the 510 was set to 0.8 µm and the zoom to 2.9. Images were 512 pixels x 100-200 pixels; 3-6 optical sections, 1 µm each, were acquired for each view. The parameters for each channel (laser intensity, brightness, contrast and gain) were set so that pixel brightness was not saturated, and were held constant during acquisition of all images for each experiment. We found no difference between results acquired with the 510 confocal microscope and the Axiovert 200, so results with the two microscopes were pooled. In all experiments, neurons were first viewed with a green-fluorescence filter and pyramidal-shaped neurons expressing GFP were imaged. Images of dendrites were acquired in two to four channels, as appropriate (Fig. 2.3). For images acquired with the Zeiss 510, Z-sections were summed and projected in the z dimension using Image J software (NIH) before analysis.

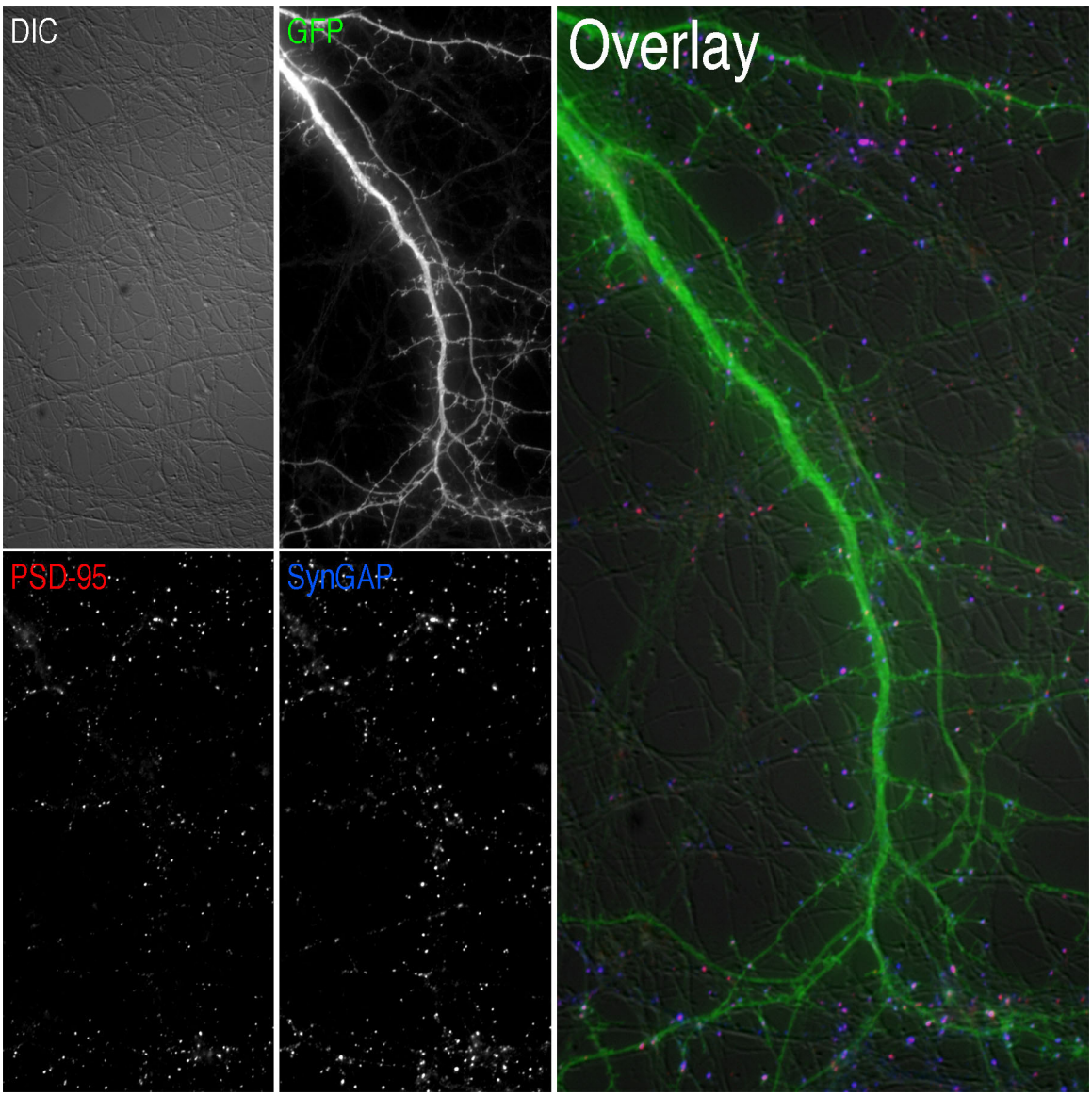

Figure 2.3: **Four-channel image of neuronal dendrites.** Representative image of neuronal dendrites obtained with a Zeiss Axiovert 200 Microscope. Fluorescence from GFP, PSD-95 and synGAP was acquired in separate channels. The presence of pure red, green and blue spots in the overlay image indicates no 'bleed-through' between channels.

2.9 Image analysis

Image analysis consisted of protrusion masking (Section 2.9.1), dendrite masking (Section 2.9.2), puncta masking (Section 2.9.3), and obtaining measurements from the resulting masked images and performing statistical analyses (Section 2.9.4). Most of this multi-step process was automated by the use of macros in KS 300 software (Zeiss). An example of such a macro is included in Appendix B.

2.9.1 Protrusion masking

Because protrusions (visualized by GFP fluorescence) are continuous with the dendritic shaft and vary enormously in shape, computer programs are poor at recognizing protrusions (Fig. 2.4A). Therefore, dendritic protrusions were manually outlined (magnetic lasso tool; Adobe Photoshop) by an investigator blinded to the genotype (Fig. 2.4B; green objects). We excluded protrusions that crossed with others, bifurcated or branched, were dim, or were longer than $\sim$6 µm (Fig. 2.4B; arrows). The resulting binary image containing only the outlined protrusions (protrusion mask) was saved for further analysis (Fig. 2.4C).

2.9.2 Dendrite masking

We also created a mask of the GFP-fluorescent dendrite (dendrite mask) using KS 300 software to exclude from analysis fluorescence from other neurons in the field. To obtain the dendrite mask, the GFP image was processed by adjusting the contrast (automatic function), high-pass filtering (mode= normalize, size= 35, count= 1), dilation (count= 6), followed by thresholding (at 125 pixel value), scrapping small objects ($<$ 10,000 pixels) and saving the binary image (Fig. 2.5A-F, respectively). We applied the dendrite mask to the corresponding images of PSD-95, synGAP, NR1, GluR1, or synapsin immunofluorescence to exclude from analysis the fluorescence from non-infected neurons in the field (Figs. 2.5G and 2.6B).

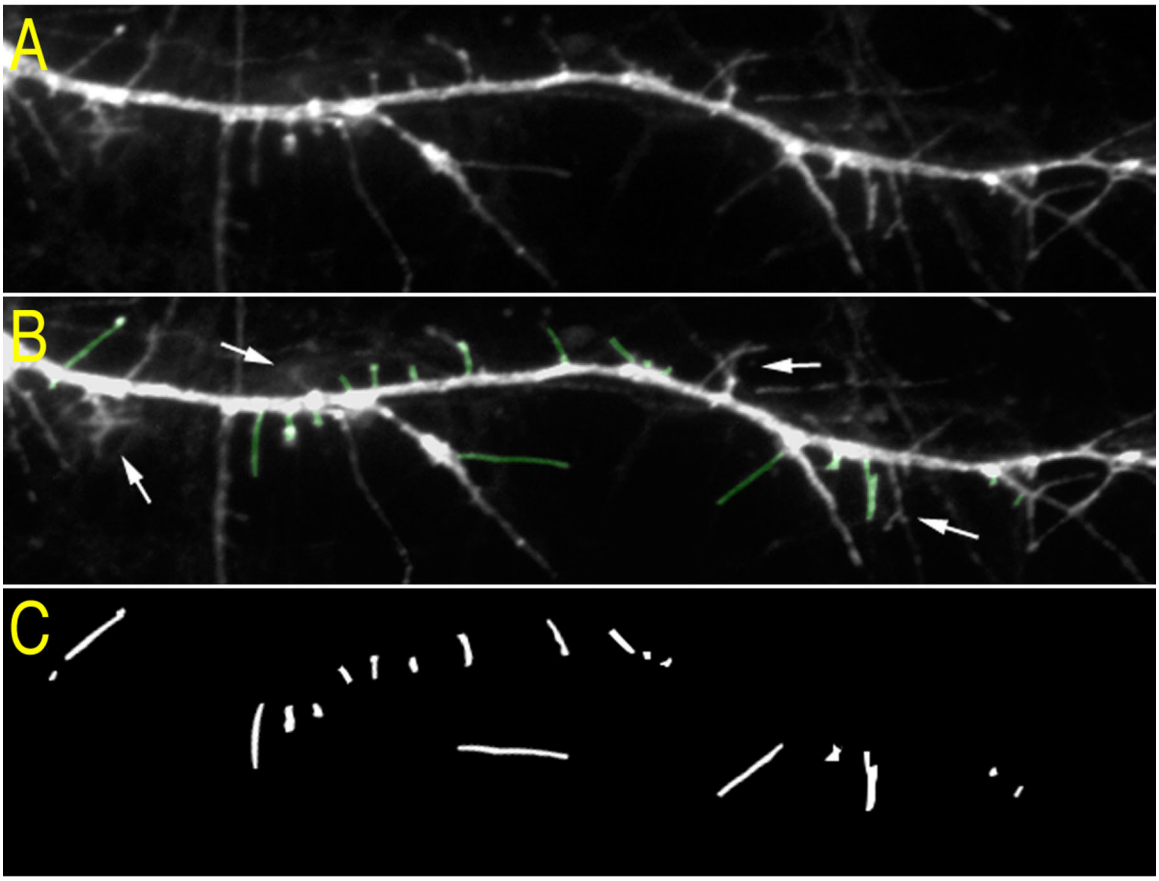

Figure 2.4: **Creating the protrusion mask.** (A) Example of a dendritic branch and protrusions visualized in the GFP-channel. (B) The selected protrusions were overlayed (green) with the GFP-channel image to display the selected protrusions. Arrows indicate protrusions that were not selected based on the criteria described in Section 2.9.1. (C) The protrusion mask.

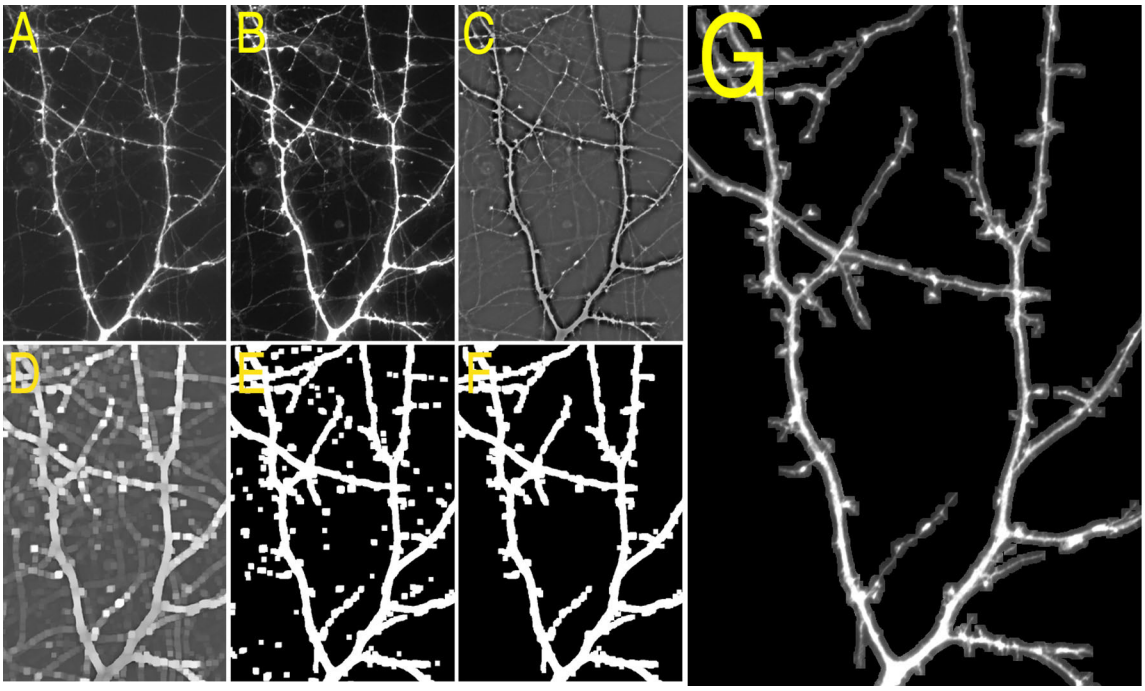

Figure 2.5: **Creating the dendrite mask.** (A) Example of a dendritic branch and protrusions visualized in the GFP-channel. (B) Contrasted image of (A). (C) High-pass filtering of (B). (D) Dilation of (C). (E)Thresholded image of (D). (F) The dendrite mask. (G) Masked image of (A).

2.9.3 Puncta masking

Fluorescence arising from immunostaining PSD-95, synGAP, NR1, GluR1 and synapsin is highly concentrated at synaptic sites. This is displayed as puncta (clusters of bright pixels) whose brightness is mostly confined within the top 95^{th} percentile of all pixels in an image (Fig. 2.6A, B). We therefore thresholded each masked image at the brightness index for the 95^{th} percentile of the pixels using KS 300 (Fig. 2.6C). In addition, we identified and separated blobs (two or more fused puncta) in the thresholded image into their component puncta by thresholding these regions at the lowest brightness value before puncta fused (see Appendix B). The resulting binary image (puncta mask) was saved for further analysis. (In an independent analysis, the threshold was kept constant for all images in an experiment, and similar results were obtained.)

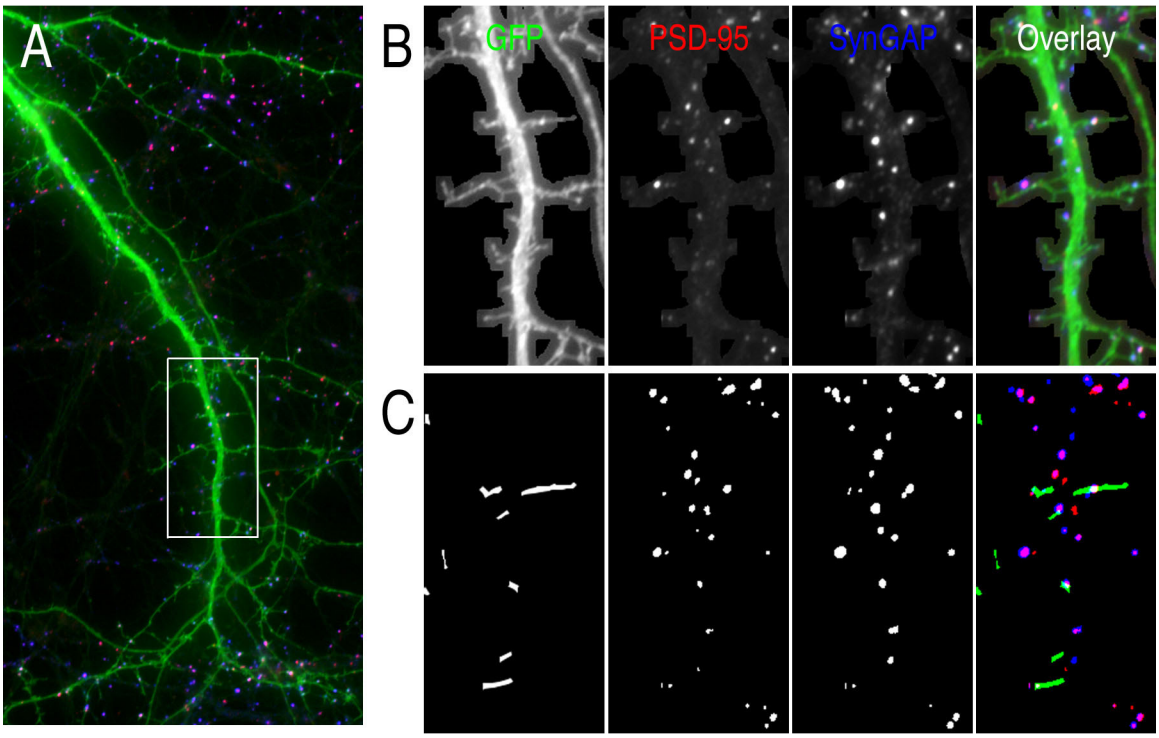

Figure 2.6: **Thresholding immunostained images.** (A) Overlay of the GFP, PSD-95 and SynGAP channels of the dendrite shown in Fig. 2.3. (B) Zoom of the boxed region shown in (A) after the dendrite mask was applied to each channel. (C) *Left*, Protrusion mask obtained from the GFP channel as described in Section 2.9.1. *Middle*, Puncta mask obtained from the PSD-95 and synGAP channels as described in Section 2.9.3. *Right*, Overlay of the protrusion mask (green) with the puncta masks of PSD-95 (red) and SynGAP (blue).

2.9.4 Measurements and statistical analyses

Using KS 300, the number of puncta and protrusions per 50 µm of dendrite, and the area and mean pixel brightness of each punctum were obtained from masked images (see Appendix B). To obtain the width of protrusions, the protrusion mask was applied to each GFP image (Fig. 2.4), then the software drew a rectangle bounding the mask around each protrusion, and the length and width of each rectangle was recorded. Note that this method of automatic analysis tends to underestimate the magnitude of differences in width of spine heads between *wt* and *ko*, because bends in filopodia increase their recorded width. To obtain the percentage of puncta in protrusions, or the percentage of protrusions containing a punctum (cluster), the intersection of the protrusion mask and the binary images of immunostained puncta was obtained (Fig. 2.6C, *right*). Then, the number of protrusions in the intersection was divided by the total number of protrusions, or the number of puncta in the intersection was divided by the total number of puncta. Values for width, area, and brightness were normalized to *wt* and all values were imported into Prism software (GraphPad, Inc., San Diego, CA) for statistical analysis and graphing. All statistical analyses were performed using unpaired Student's t-test or one-way ANOVA, as indicated. Significance was accepted as $P < 0.05$.

Although synGAP^{wt} was constructed with a FLAG-tag at the amino terminus, we were unable to detect the tag by immunocytochemistry. Therefore, to estimate the expression of synGAP in neurons infected with Sindbis virus expressing recombinant synGAP, we applied the dendrite mask (described above) to the images of synGAP fluorescence in infected neurons. We measured the mean brightness of synGAP fluorescence within the dendrite mask (total brightness / area). We corrected these values by subtracting the mean brightness of *ko* neurons. Corrected average values for neurons expressing recombinant synGAP were normalized to the corrected average value for *wt*.

2.10 Electrophysiological recordings

Hippocampal neurons were maintained in culture for 10 days. Physiological recordings were performed by Irina Sokolova in Henry Lester's laboratory. Miniature excitatory postsynaptic currents (mEPSCs) were recorded with a patch electrode (4-5 M) in the whole-cell voltage clamp mode (Axopatch 200, Axon Instruments) (Fig. 2.7).

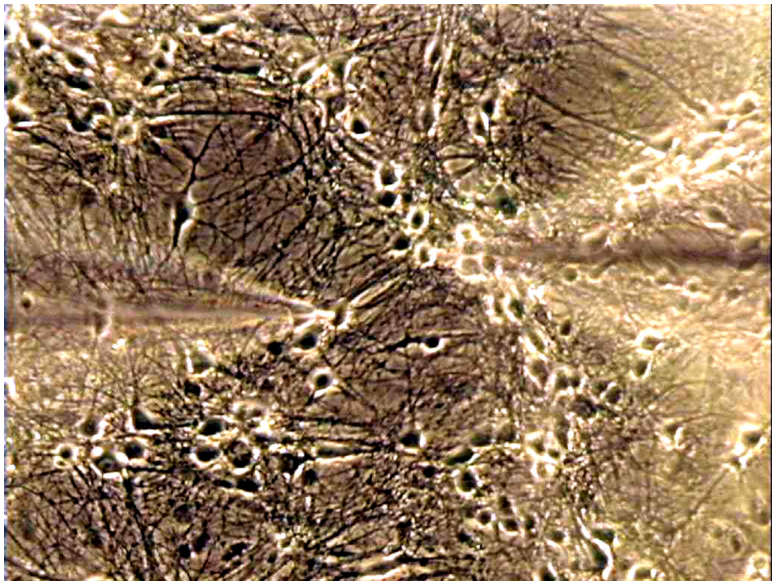

Figure 2.7: **Recording miniature excitatory postsynaptic currents (mEPSCs).** Image of the setup used for recording mEPSCs from hippocampal cultures. We patched one to two cells and recorded mEPSCs for ∼3 min at room temperature.

The bathing solution contained (in mM): NaCl 145, KCl 5, $MgCl_2$ 0.5, $CaCl_2$ 2, HEPES 5, glucose 10, pH 7.4. Glutamatergic mEPSCs were pharmacologically isolated by adding tetrodotoxin (0.5 µM) and picrotoxin (30 µM) to the bath solution. The pipette solution contained (in mM): potassium gluconate 145, KCl 10, NaCl 5, $MgCl_2$ 2, $CaCl_2$ 0.1, EGTA 5, HEPES 5, ATP 2, pH 7.2. Recordings of mEPSCs were obtained for 3 min at a potential of -70 mV. Access resistance (15-18 M) of the electrode was measured throughout the recordings and did not change more than 10%. Records were filtered at 2 kHz and digitized at 10 kHz. Parameters of mEPSCs were analyzed with custom made software. Asymmetric events with a rise time shorter than the decay time and amplitude greater than 4 pA (the threshold for event detection)

were chosen for the analysis. Data were acquired from 10 *wt* and 9 *ko* neurons arising from 3 and 2 different embryos, respectively. Data from each group were averaged, and statistical significance of differences of means was determined by unpaired Student's t test.

Chapter 3

Results

3.1 Generation and phenotype of synGAP *ko* mice

ES cells were transfected with a targeting construct that contained three loxP sites enclosing a neomycin selection cassette and genomic DNA including exons 4 through 9 of synGAP (Fig. 3.1A). After selection for homologous recombination, mutant ES cells were transfected with a vector that transiently expresses Cre-recombinase (see Section 2.1). We screened these ES cells for mutants with a complete deletion of exons 4 through 9 (*ko*). Two distinct ES cell colonies bearing the *ko* mutation were used to develop two independent lines of synGAP *ko* mice. Both of the lines express the same phenotypes and we use them interchangeably. The genotype of individual mice is determined by polymerase chain reaction of genomic DNA (Fig. 3.1B) as described in Section 2.3.

The synGAP *ko* mutation results in a recessive lethal phenotype. On postnatal day 0 (P0), homozygous *ko* mice are initially similar in size to *wt* and a milk spot is often observed in their abdomens, suggesting that mortality is not caused by immediate malnutrition. Blood sugar levels are similar among littermates (data not shown). However, the *ko* mice rapidly develop a 'failure to thrive' phenotype. They do not grow well and by P1 become noticeably smaller than their littermates. They begin to weaken, display impaired motor skills and trembling, and generally die on P1 or by early P2. In contrast, cultured neurons derived from *ko* embryos appear healthy *in vitro* and are indistinguishable by phase microscopy from cultured neurons derived

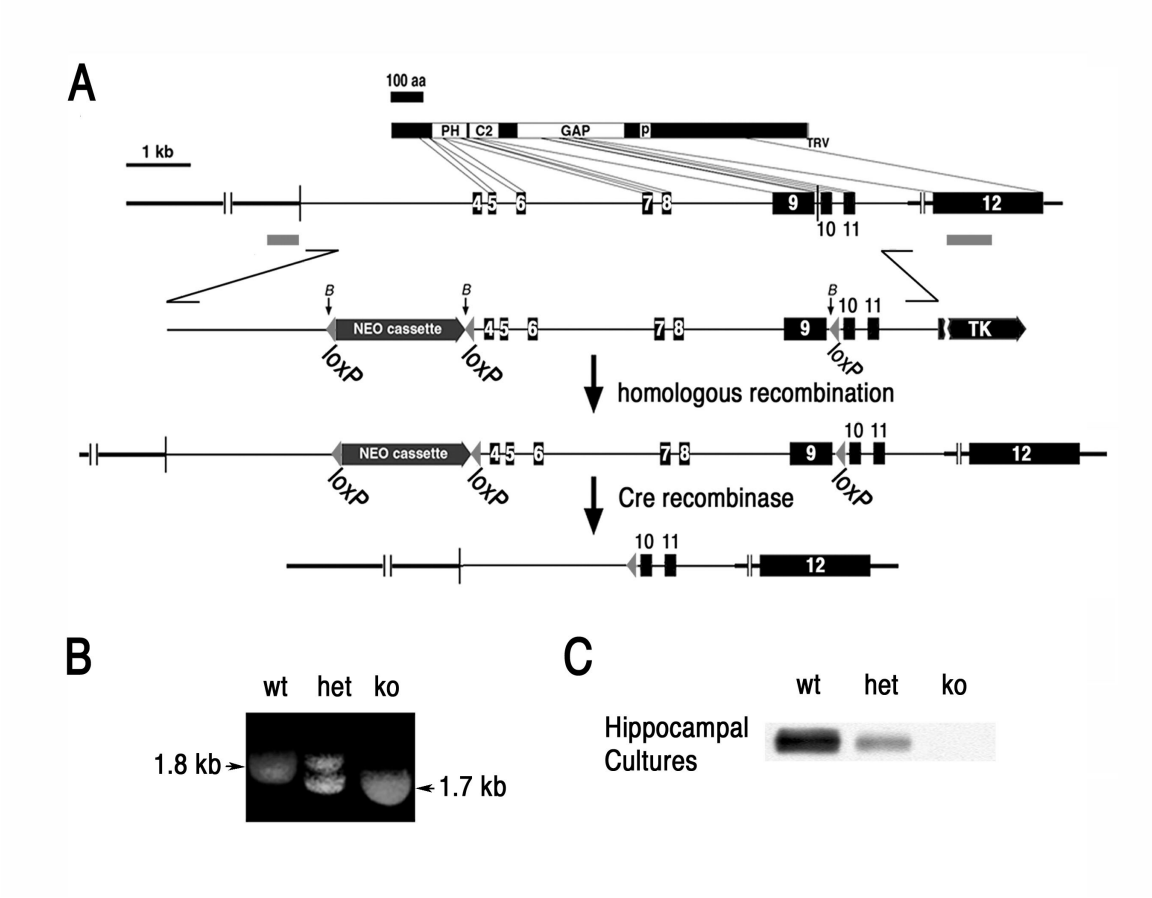

Figure 3.1: **Generation of a synGAP *ko* mouse.** (A) The targeting construct included a Neo cassette flanked by Lox P sites inserted into intron 3 of the synGAP gene, and an additional downstream Lox P site within intron 9. Expression of Cre recombinase in recombinant ES cells resulted in deletion of exons 4-9 of the synGAP gene (*ko*) in a subset of ES cells, two of which were used to construct synGAP *ko* lines. (B) Example of PCR products from DNA of *wt*, *het*, and *ko* embryos. (C) Immunoblots comparing synGAP levels in hippocampal neurons cultured from *wt*, *het*, and *ko* embryos, as described under Experimental Procedures. Expression of all four isoforms of synGAP protein is absent in *ko* neurons and reduced in *het* neurons compared to *wt*.

from *wt* littermates (Fig. 2.1B). The neurons display levels of synGAP expected from their genotype (Fig. 3.1C). Heterozygous neurons have about half as much synGAP and synGAP is not detectable in homozygotes.

3.2 Spine morphology in neuronal cultures

To investigate whether absence of synGAP has an effect on dendritic spines, we examined the size and the number of dendritic spines in dissociated hippocampal neurons cultured from individual E16 or E17 embryos. To accomplish this, we imaged 21 DIV neurons filled with heterologously expressed GFP (see Section 2). We found that spines are significantly larger in synGAP *ko* neurons (Fig. 3.2A and B). *Ko* neurons have spines with a mean head width 1.2 times larger, and mean area 1.34 times larger, than those in *wt* neurons (Fig. 3.2B). However, we did not find significant differences in the density of spines per dendrite (15.5 $\pm$ 0.6 vs *ko* in *wt* vs. 16.2 $\pm$ 0.8 in *ko* neurons).

Similarly, PSD-95 immunostained puncta are also larger and brighter in synGAP *ko* neurons (Fig. 3.2A and C). Thus, absence of synGAP leads to enlarged spines in mature neurons in culture.

3.3 Development of spines in neuronal cultures

Defects in spine formation and maturation can give rise to the enlarged spines observed in 21 DIV synGAP *ko* neurons. To investigate whether loss of synGAP affects the maturation of spines in culture, we examined spine formation in dissociated hippocampal neurons cultured from individual E16 or E17 embryos. We found that mature looking spines appear earlier on dendrites of *ko* neurons than on those of *wt* neurons. We examined the morphology of dendritic protrusions on pyramidal shaped neurons (Fig. 3.3A) at 10 DIV, by imaging neurons filled with heterologously expressed GFP (see Section 2.7). There is a small increase in the number of protrusions on dendrites of *ko* neurons compared to *wt*. However, the more dramatic change

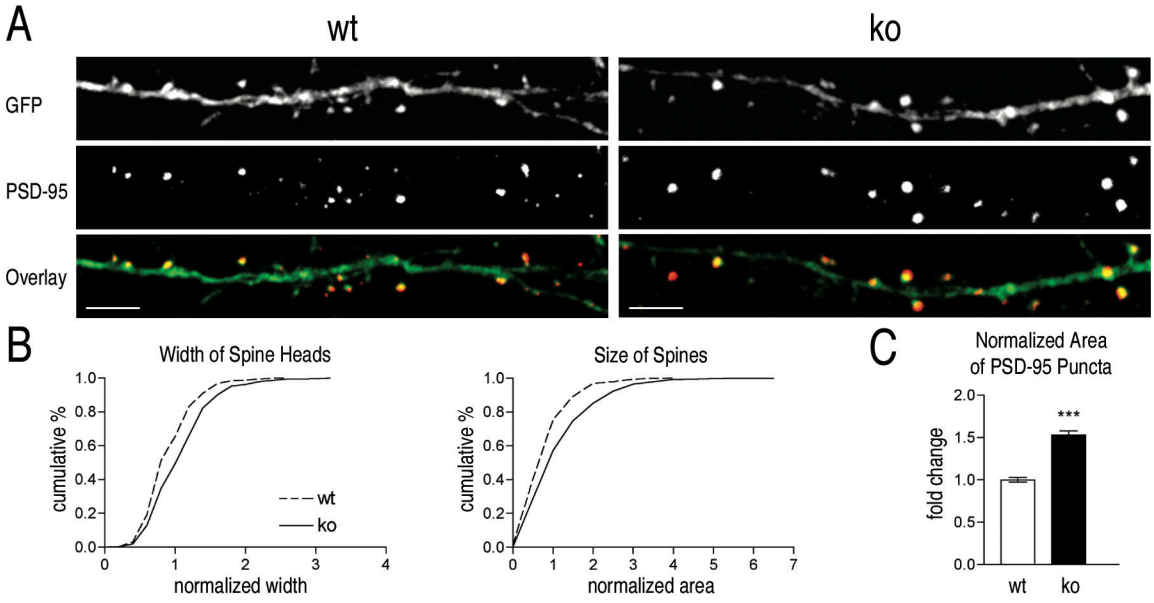

Figure 3.2: **21 DIV synGAP *ko* neurons have larger dendritic spines.** (A) Representative confocal images of projected z-sections of 50 µm dendritic segments from cultured hippocampal neurons on 21 DIV. *Upper*, GFP was expressed for 18 h to outline the dendritic morphology (see Section 2). Spines in mature *ko* neurons are larger than spines in mature *wt* neurons. *Middle*, Neurons were immunostained for PSD-95. PSD-95 immunostained puncta are larger and brighter in *ko* neurons. *Lower*, Overlay of GFP and PSD-95. Scale bar, 5 µm. (B) Quantification of width and area of spines at 21 DIV. Both widths and areas of spines are shifted towards larger values in *ko* neurons compared to *wt* neurons. Width of spines (mean ± sem); *wt*, 1.0 ± 0.01 vs *ko*, 1.2 ± 0.01, $P < 0.0005$. Area of spines; *wt*, 1.0 ± 0.02 vs *ko*, 1.34 ± 0.03; $P < 0.0005$. (C) Quantification of area of PSD-95 puncta at 21 DIV. Area of PSD-95 puncta (mean ± sem); *wt*, 1.0 ± 0.03 vs *ko*, 1.5 ± 0.05, $P < 0.0005$. Measurements were made of 876 protrusions and 3,090 PSD-95 puncta on 57 dendrites from 13 *wt* neurons and 881 protrusions and 2,533 PSD-95 puncta on 54 dendrites from 15 *ko* neurons. Some PSD-95 puncta included in the analysis belonged to other 'GFP-lacking' dendrites in the field.

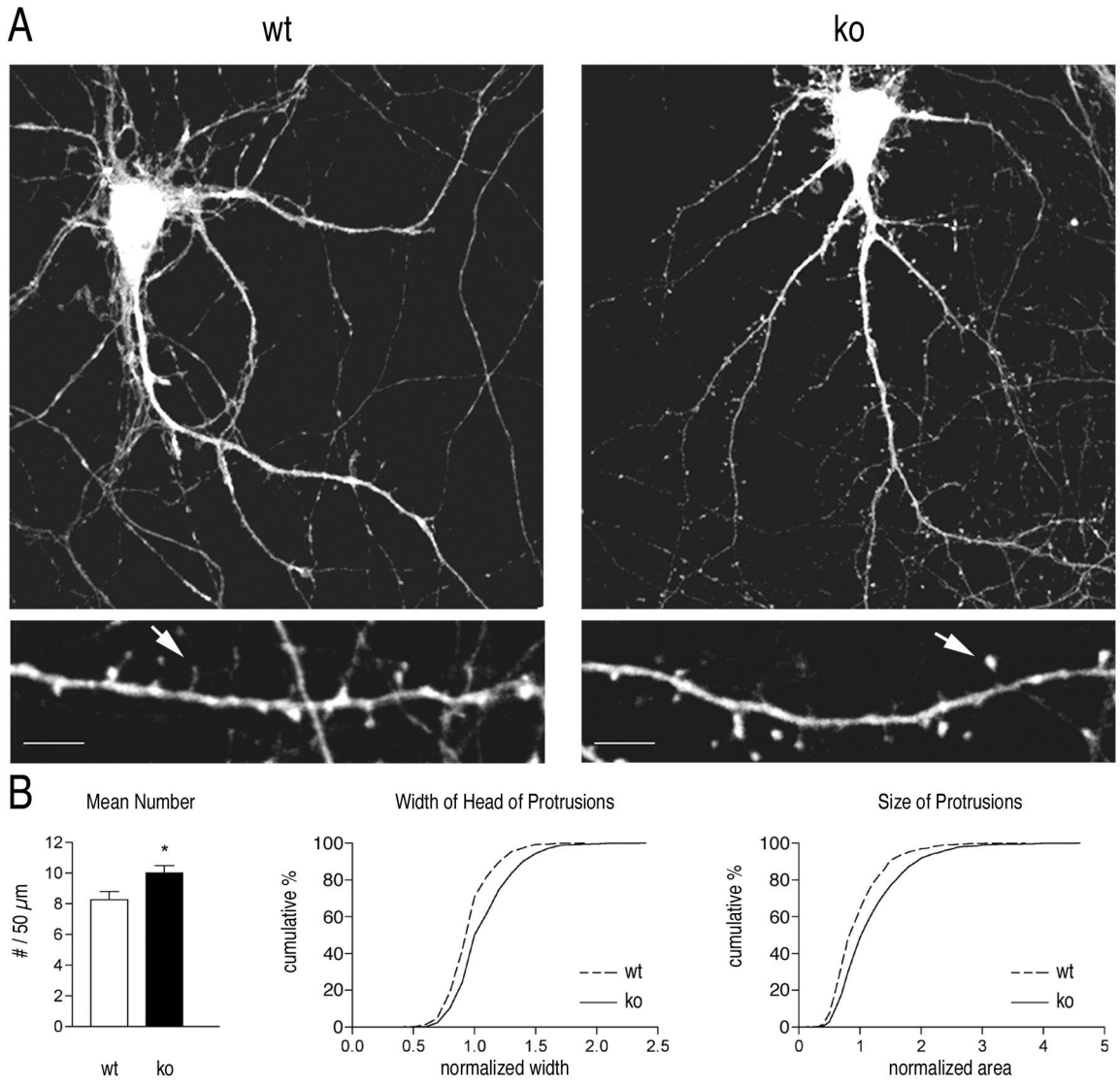

Figure 3.3: **SynGAP *ko* neurons have larger dendritic protrusions.**(A) *Top*: Representative confocal images of cultured hippocampal neurons at 10 DIV after expression of eGFP on 9 DIV (see Section 2.7). *Bottom*: Projected z-sections of dendritic segments (50 µm long) imaged by confocal microscopy. The population of protrusions on dendrites of *ko* neurons is shifted toward those with large heads resembling mature spines, compared to the distribution of protrusions on dendrites of *wt* neurons. In *wt* neurons, thinner, elongated filopodia predominate (see arrows). Scale bar, 5 µm. (B) Quantification of number, width, and area of dendritic protrusions at 10 DIV. The number of protrusions in projected z-sections of 50 µm dendritic segments increased from 8.27 ± 0.52 in *wt* (n = 79) to 10.00 ± 0.48 in *ko* (n = 87, *p = 0.016). Widths and areas of protrusions normalized to *wt* are represented as cumulative histograms with bins of 0.2 normalized units. Both width and area are shifted towards higher values in *ko* neurons (width (mean ± sem); *wt*, 1.00 ± 0.01 vs. *ko*, 1.12 ± 0.01, $P < 0.0005$: area (mean ± sem); *wt*, 1.00 ± 0.02 vs. *ko*, 1.22 ± 0.02, $P < 0.0005$). Note that the automated measurement of width underestimates the differences in head width between *wt* and *ko* (see Section 2.9.4). Measurements were made of 653 protrusions on 79 dendrites from 29 *wt* neurons and 870 protrusions on 87 dendrites from 27 *ko* neurons.

is a shift in the distribution of morphologies of the protrusions toward that of mature spines with wide heads (Fig. 3.3A, *right*), and away from that of thin filopodia (Fig. 3.3A, *left*; (Fig. 3.3B). Thus, some of the alterations in spine structure observed in *ko* mature neurons (21 DIV) arise during synapse formation (at 10 DIV).

3.4 Synaptic proteins

The hypothesis that spine maturation occurs earlier in *ko* neurons than in *wt* is supported by the sizes of clusters and subcellular distributions of postsynaptic proteins. Clusters of PSD-95 are present in dendrites of both *wt* and *ko* neurons (Fig. 3.4A, Top); however, the clusters are significantly larger in *ko* neurons (Fig. 3.4B). The same is true for clusters of subunits of the NMDA-type (NR1) and AMPA-type (GluR1) glutamate receptors (Fig. 3.4A, Bottom; (Fig. 3.4B). Individual clusters of these proteins are also brighter in *ko* neurons (NR1, 1.10 $\pm$ 0.02 fold; GluR1, 1.49 $\pm$ 0.02 fold; PSD-95, 1.35 $\pm$ 0.02 fold), supporting the interpretation that, on average, each cluster in *ko* neurons contains more protein. In contrast, the areas of clusters of the presynaptic protein synapsin are only slightly altered in *ko* neurons (Fig. 3.4A, B).

The numbers of clusters of PSD-95, NR1, and GluR1 in dendrites are approximately the same in *wt* and *ko* neurons at 10 DIV; however, in *ko* neurons, many more of the clusters are located at the tips of protrusions than in *wt* (Fig. 3.5). Similarly, a larger proportion of protrusions in *ko* neurons contain a cluster of PSD-95 than in *wt* neurons at this age (Fig. 3.6A), and more of these protrusions are associated with a presynaptic synapsin puncta, indicating the presence of a synaptic junction. Finally, more protrusions in *ko* neurons contain both AMPA-type and NMDA-type glutamate receptors as opposed to NMDA-type receptors alone (Fig. 3.6B). Thus, by this criterion, the proportion of 'silent' synapses is reduced in *ko* neurons compared to *wt* neurons at 10 DIV. Taken together, these data show that at 10 DIV, the population of protrusions in *ko* neurons has shifted substantially toward a mature spine phenotype when compared to *wt* neurons.

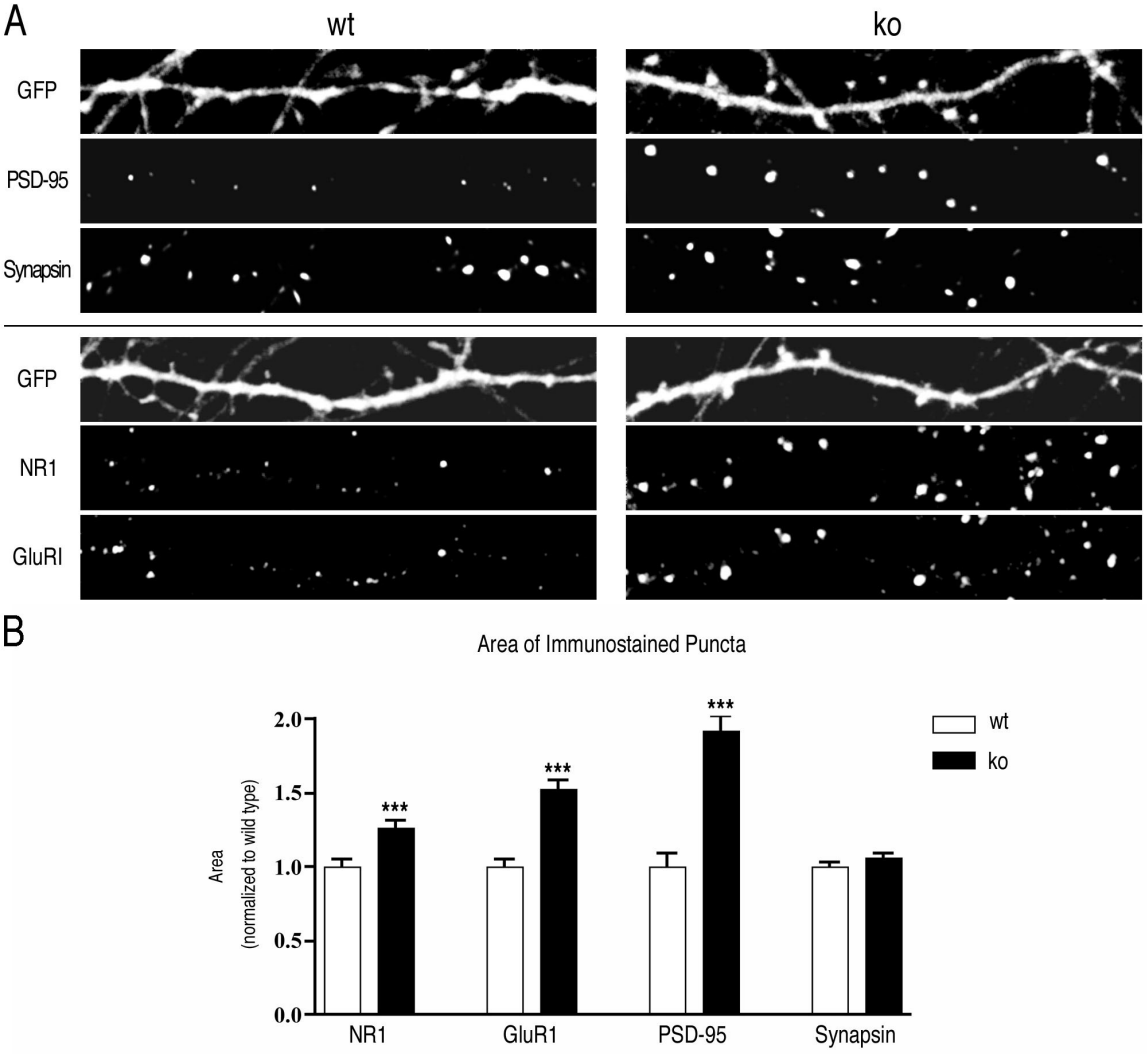

Figure 3.4: **Clusters of postsynaptic proteins are larger in *ko* neurons.** (A) Representative images of dendritic segments (50 µm long) from eGFP-expressing *wt* and *ko* neurons at 10 DIV prepared as described in Fig. 3.3), and immunostained for PSD-95, and synapsin (*top*), or for NR1 and GluR1 (*bottom*), as described under Section 2.5. PSD-95, NR1, and GluR1 immunostained puncta are larger in *ko* neurons. Scale bar, 5 µm. (B) Areas of immunostained puncta. Images were masked and thresholded as described in Section 2.9. The mean areas of puncta in *ko* neurons were normalized to those of *wt* puncta. Area of NR1 puncta: *wt*, 1.00 ± 0.05; *ko*, 1.26 ± 0.05. Area of GluR1 puncta: *wt*, 1.00 ± 0.06; *ko*, 1.53 ± 0.06. Measurements were made of 506 NR1 puncta and 651 GluR1 puncta on 43 dendrites from 13 *wt* neurons, and of 605 NR1 puncta and 666 GluR1 puncta on 52 dendrites from 12 *ko* neurons. Area of PSD-95 puncta: *wt*, 1.00 ± 0.09; *ko*, 1.92 ± 0.10. Area of synapsin puncta: *wt*, 1.00 ± 0.03; *ko*, 1.06 ± 0.04 (P = .228). Measurements were made of 264 PSD-95 puncta and 992 synapsin puncta on 36 dendrites from 16 *wt* neurons, and 246 PSD-95 puncta and 712 synapsin puncta on 35 dendrites from 12 *ko* neurons. (***p $<$ 0.0005; two-tailed Student's t-test).

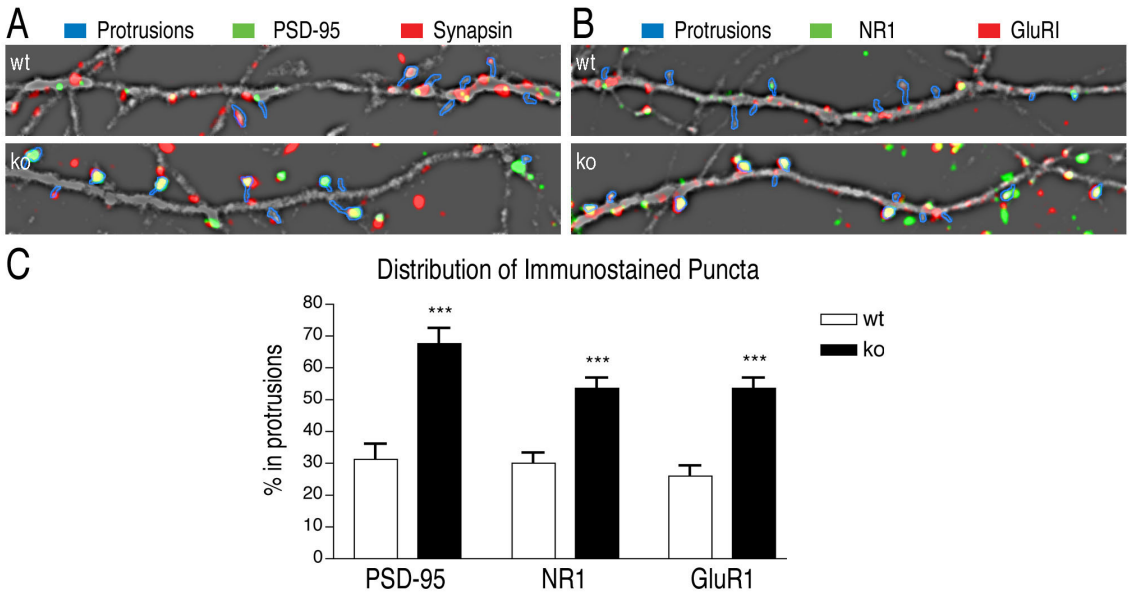

Figure 3.5: **At 10 DIV, more clusters of postsynaptic proteins have moved into protrusions in *ko* neurons than in *wt* neurons.** (A) Images from Fig. 3.4A (*top*) have been overlayed to illustrate locations of PSD-95 and synapsin-labeled puncta. The GFP image was made translucent with a highpass filter for a better view of the distribution of PSD-95 (green) and synapsin (red) in dendrites. Protrusions were outlined by hand (blue for clarity). (B) Images from Fig. 3.4A (*bottom*) have been overlayed and displayed as in (A) to illustrate locations of NR1 and GluR1-labeled puncta. (C) At 10 DIV, a larger percentage of postsynaptic proteins have moved from the dendritic shaft into protrusions in *ko* neurons than in *wt* neurons. From the data described in Fig. 3, we measured the percent of PSD-95, NR1 and GluR1 puncta that overlap with dendritic protrusions as defined by the protrusion mask described in Section 2.9.4. Percent of PSD-95 clusters in protrusions (mean ± sem): *wt*, 31.3 ± 4.6; *ko*, 67.8 ± 4.6. NR1 in protrusions: *wt*, 26.0 ± 3.1; *ko*, 53.5 ± 3.4. GluR1: *wt*, 30.0 ± 3.3; *ko*, 53.6 ± 3.3. Measurements were made on the same set of data analyzed in Fig. 3.4. (***p < 0.0005, Students t-test.)

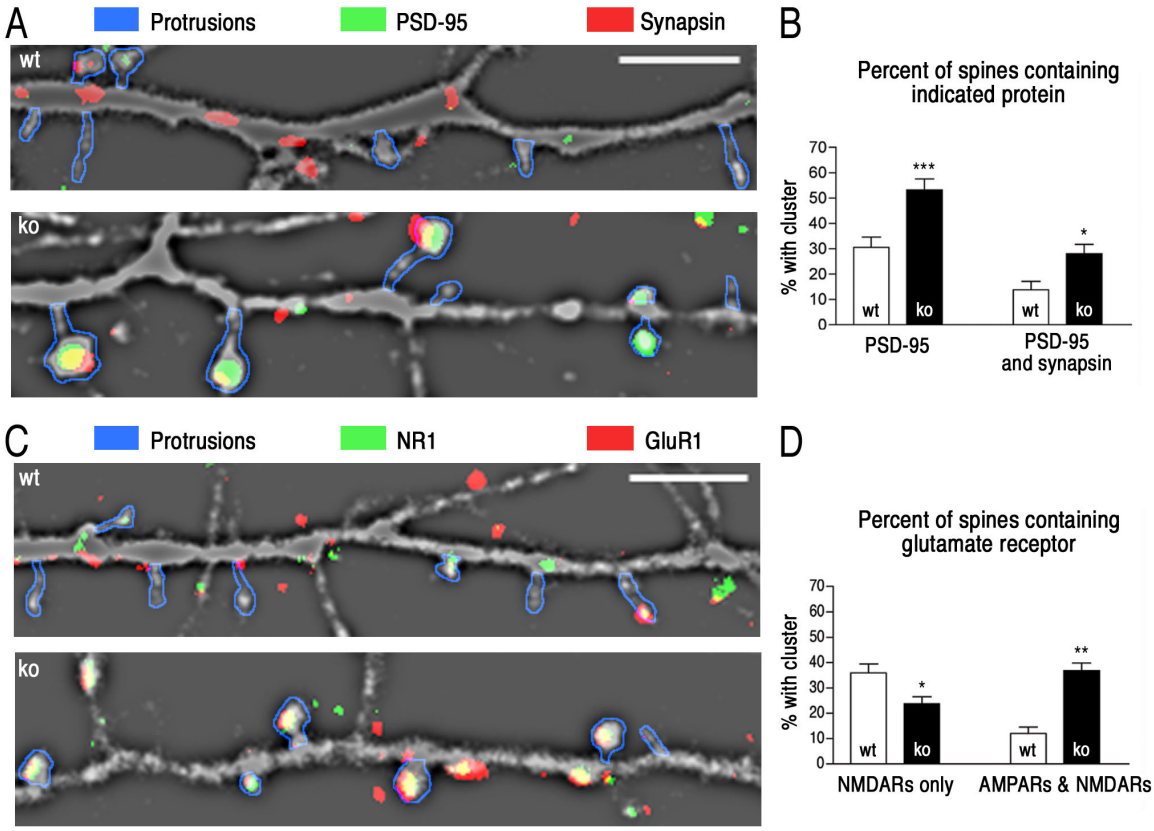

Figure 3.6: **At 10 DIV, more protrusions on *ko* neurons have characteristics of mature spines than on *wt* neurons.** (A) In *ko* neurons, more spines have a cluster of PSD-95 associated with a presynaptic terminal indicated by a synapsin puncta. Representative images of dendrites stained for PSD-95 (green) and synapsin (red) are presented as in Fig. 3.4. Immunostained puncta were identified as in Fig. 3.5. (B) The percentage of protrusions overlapping with a PSD-95 puncta or with both a PSD-95 puncta and a synapsin puncta was determined as described in Section 2.9.4. The percentage of protrusions containing PSD-95 increased from 30.5 ± 4.1 % in *wt* neurons to 53.2 ± 4.4 % in *ko* neurons. The percentage containing both PSD-95 and synapsin increased from 14 ± 3.4 % in *wt* neurons to 28.0 ± 3.7 % in *ko* neurons. Measurements were made on the same set of data analyzed in Fig. 3.4. (C) In *ko* neurons, more spines contain both AMPA and NMDA-type glutamate receptors than contain NMDA-type receptors alone. Representative images of dendrites stained for NR1 (green) and GluR1 (red) are presented as in Fig. 3.5. Immunostained puncta were identified as in Fig. 3.4. (D) The percentage of protrusions containing only NMDA receptors decreased from 36 ± 3.5 % in *wt* neurons to 24 ± 2.8 % in *ko* neurons. Conversely, the percentage of spines containing both AMPA and NMDA receptors was greater in *ko* neurons (37 ± 3.0 %) than in *wt* neurons (12 ± 2.5 %). Measurements were made on the same set of data analyzed in Fig. 3.4. (* $p < 0.01$, ** $p < 0.005$, *** $p < 0.0005$, Student's t-test.)

3.5 Miniature excitatory postsynaptic currents in neuronal cultures

The morphological characteristics of *ko* neurons at 10 DIV suggest that they have more active synapses than *wt* neurons at the same age. To test this hypothesis, we compared the frequency and amplitude of miniature excitatory postsynaptic currents (mEPSCs) in *ko* neurons to those in *wt* neurons at 10 DIV (Fig. 3.7). We found a higher frequency of mEPSCs in the *ko* neurons (Fig. 3.7C), confirming that more synaptic terminals release glutamate onto receptor clusters in *ko* neurons than in *wt* neurons at this age. In addition, the amplitude of the mEPSCs in *ko* neurons was considerably larger than in *wt* neurons, indicating that physiologically responsive glutamate receptor clusters are larger at synapses in *ko* neurons (Fig. 3.7A and B).

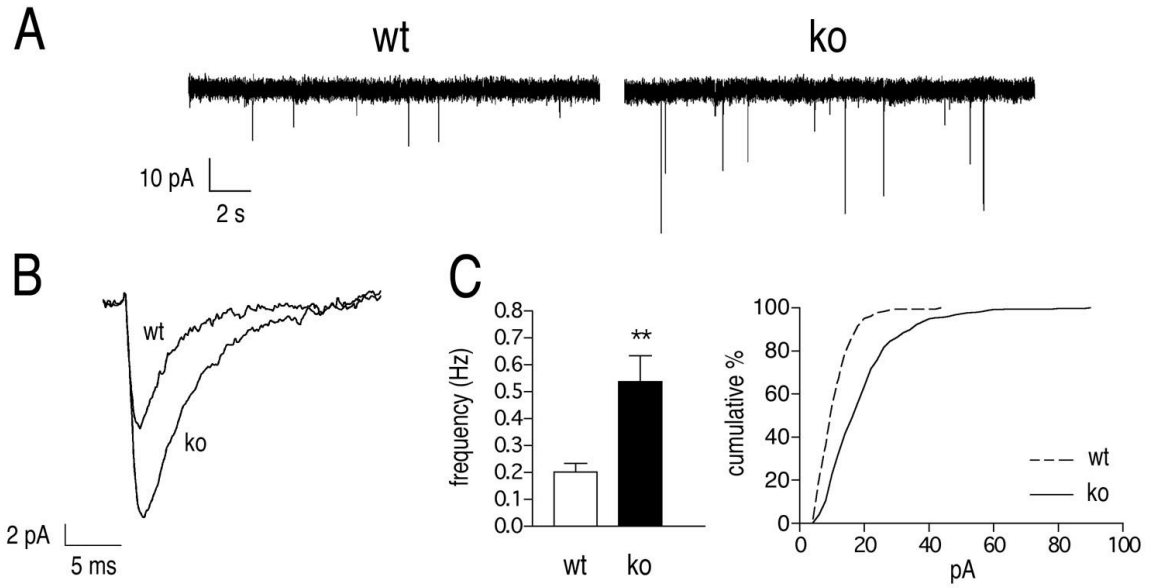

Figure 3.7: **Frequency and amplitude of mEPSCs are increased in cultured synGAP *ko* neurons at 10 DIV.** (A) Representative electrophysiological traces of spontaneous synaptic activity in *wt* and *ko* neurons. Three min long recordings of mEPSCs were obtained at a potential of -70 mV. (B) Averaged mEPSCs illustrating the increase in peak amplitude in *ko* neurons compared to *wt* controls. (C) Frequencies and peak amplitudes of mEPSCs. The mean frequency was higher in *ko* neurons (*wt*, 0.2 ± 0.03 Hz vs *ko*, 0.5 ± 0.1 Hz, **p < 0.005). The entire distribution of mEPSC amplitudes shown in the cumulative histogram is shifted to higher values in *ko* neurons (*wt*, 11.7 ± 0.5 pA vs *ko*, 19.8 ± 0.5 pA, ***p < 0.0001). Measurements were made of 181 mEPSCs from 10 *wt* neurons and 435 mEPSCs from 9 *ko* neurons isolated from 3 *wt* embryos and 4 *ko* embryos.

3.6 Reintroduction of synGAP into *ko* neurons

To reintroduce synGAP protein, and other mutant versions of synGAP protein, into *ko* neurons, we infected *ko* neurons with Sindbis viruses engineered to independently express GFP and synGAP (Section 2.7). Using an IRES2 promotor to drive the expression of recombinant synGAP, we achieved expression levels comparable to those of endogenous synGAP in *wt* neurons (Fig. 3.8). There is a slight increase in the size of recombinant synGAP puncta, relative to endogenous synGAP in *wt* neurons (Fig. 3.8C). This is probably due to the increased size of spines in *ko* neurons.

Targeting of synGAP to dendritic spines was indistinguishable between endogenous synGAP in *wt* neurons and recombinant synGAP in *ko* neurons (Fig. 3.8A and B, *left*). This targeting was unaffected either by mutating the GAP domain of synGAP (GAP^{mut}) (Fig. 3.8B), *middle*), or deleting the t-T/SXV motif of synGAP (ΔSXV) (Fig. 3.8B), *right*). This surprising finding suggests that binding to PSD-95 is not necessary to target synGAP to dendritic spines. However, the percent overlap of a synGAP punctum by a PSD-95 punctum is significantly less when synGAP lacks its t-T/SXV motif (Fig. 3.8C). Even though differences in the size of puncta indeed influence the percent overlap of a synGAP punctum by a PSD-95 punctum, the size of synGAP or PSD-95 puncta (not shown) were not different among the recombinant synGAP proteins (Fig. 3.8C). This suggests that the 'micro-localization' of ΔSXV within spines might be altered.

We also noticed that 5–10 % of the neurons infected with the GFP-IRES-SynGAP Sindbis virus (Section 2.7) expressed either GFP or synGAP alone (Fig. 3.9). Expression of only one protein from the Sindbis bicystronic RNA could result from mRNA degradation, or formation of secondary structures in the RNA which may interfere with viral RNA replication or the neuronal translational machinery. Alternatively, some viruses could have been packaged with incomplete RNA genomes. We did not explore the cause of this altered expression and disregarded neurons expressing only one recombinant protein from our analysis. Nevertheless, these rare cases indicated that expression of *wild-type* synGAP ($synGAP^{wt}$) was necessary to rescue the ab-

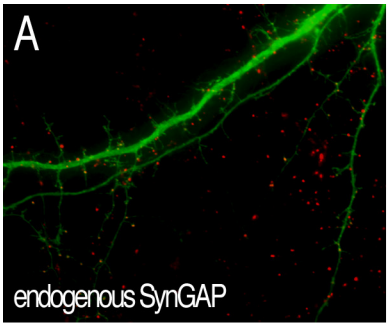

C

	wt (endogenous)	*ko* + SynGAP^{wt}	*ko* + GAP^{mut}	*ko* + ΔSXV
SynGAP brightness in dendrites	100	93 ± 9.4	89 ± 16.0	126 ±13.4
Size of SynGAP puncta	100 ± 0.9	110 ± 1.2	115 ± 1.4	109 ± 1.5
% synGAP-PSD95 puncta overlap	69.9 ± 0.4	55.2 ± 0.6	56.7 ± 0.6	46.3 ± 0.9

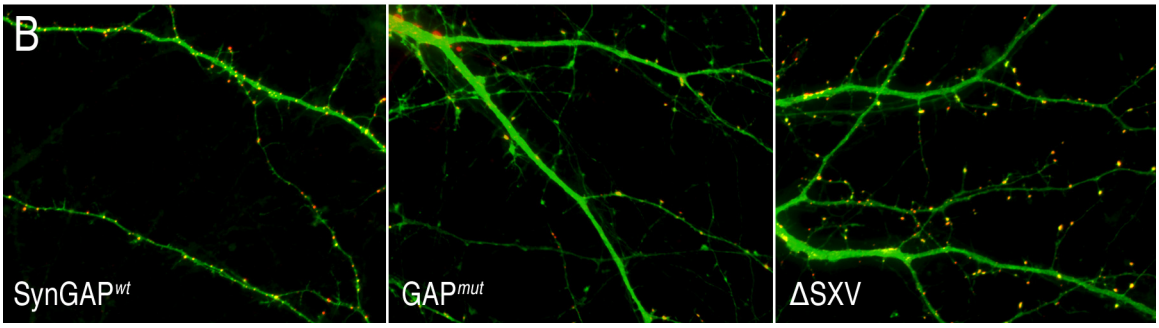

Figure 3.8: **Expression of recombinant synGAP in 10 DIV *ko* neurons.** (A) Representative image of a *wt* neuron expressing GFP (green) and stained at 10 DIV with antibodies against synGAP (red). This image shows endogenous distribution and brightness of synGAP. (B) Representative images of synGAP *ko* neurons that were infected at 9 DIV with Sindbis viruses engineered to express the GFP (green) and either synGAP^{wt} (*left*), GAP^{mut} (*middle*) or ΔSXV (*right*) as described in Section 2.7. Neurons were fixed at 10 DIV and stained with antibodies against synGAP (red). (C) Quantification of synGAP brightness in dendrites, Area of synGAP puncta, and percent overlap of a synGAP punctum by a PSD-95 punctum. Measurements were made of 10,474 synGAP puncta and 7,089 synGAP/PSD-95-overlapping puncta on dendrites from 31 *wt* neurons, 7,980 synGAP puncta and 3,179 synGAP/PSD-95-overlapping puncta on dendrites from 32 *ko* neurons expressing synGAP^{wt}, 6,011 synGAP puncta and 2,794 synGAP/PSD-95-overlapping puncta on dendrites from 22 *ko* neurons expressing GAP^{mut}, and 4,093 synGAP puncta and 1,330 synGAP/PSD-95-overlapping puncta on dendrites from 17 *ko* neurons expressing ΔSXV.

normal spine phenotype of 10 DIV synGAP *ko* neurons (Fig. 3.9). We analyze the extent of rescue in Section 3.7.

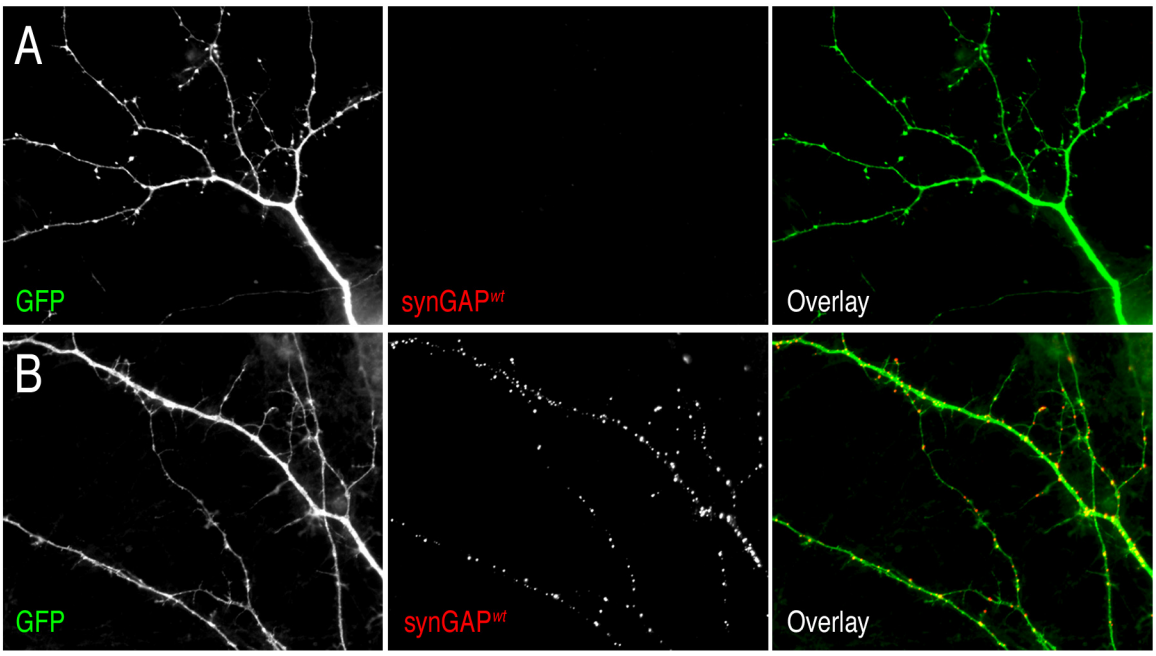

Figure 3.9: **Transient expression of synGAP apparently rescues precocious spine maturation in *ko* neurons at 10 DIV.** SynGAP *ko* neurons were infected at 9 DIV with Sindbis viruses engineered to express the GFP and synGAP, as described in Section 2.7. Neurons were fixed at 10 DIV and stained with antibodies against synGAP. Although infected, the neuron in (A) did not express recombinant synGAP^{wt} encoded in the Sindbis bicystronic RNA. As indicated by the GFP images, the *ko* abnormal spine phenotype was only rescued in neurons where synGAP^{wt} was expressed (B).

3.7 Rescue of the mutant phenotype by recombinant *wild-type* synGAP

To test whether altered spine maturation in the *ko* neurons could be reversed by transient expression of *wild-type* synGAP (synGAP^{wt}), we compared neurons infected at day 9 with Sindbis virus engineered to express both synGAP^{wt} and GFP, or GFP alone. By 18 h after infection (day 10), *ko* neurons contained, on average, the same levels of synGAP as *wt* neurons, although the levels of expression were highly variable (Fig. 3.10, 3.11E). The reintroduction of synGAP into *ko* neurons shifted

the appearance of protrusions toward that of *wt* neurons (Fig. 3.9 and 3.10). The mean width of protrusions decreased from 1.140 ± 0.085 fold to 1.027 ± 0.023 fold of *wt* (Fig. 3.10, 3.11F). In addition, the percentage of protrusions that contained a cluster of PSD-95 was reduced from 46.5 ± 2.8 % in *ko* neurons back to 28.5 ± 2.5 %, the same level as in *wt* neurons (Fig. 3.10, 3.11G). This result indicates either that the process of spine maturation is highly dynamic and thus largely reversible in less than 18 h, or that the process began at about the same time that expression of recombinant synGAP reached significant levels.

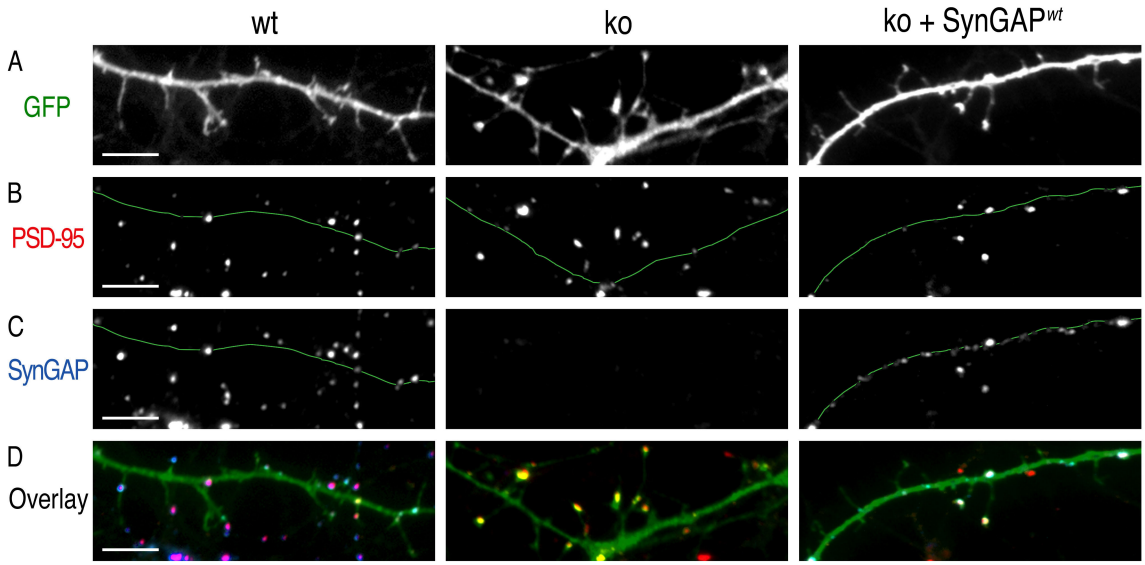

Figure 3.10: **Transient expression of synGAP partially rescues precocious spine maturation in hippocampal neurons at 10 DIV.** Cultured hippocampal neurons were infected at 9 DIV with Sindbis viruses engineered to express the indicated proteins, as described in Section 2.7. Neurons were fixed at 10 DIV and stained with antibodies against PSD-95 and synGAP. Quantitative analysis of the data from which the images are taken is shown in Fig. 3.11. (A) Representative images of dendritic segments from *wt* neurons expressing GFP, *ko* neurons expressing GFP, and *ko* neurons expressing both GFP and synGAP^{wt}. Transient expression of synGAP in *ko* neurons shifts the appearance of dendritic protrusions back toward that of *wt*. (B) Immunostaining for PSD-95 in the dendritic segments shown in (A). The location of the dendritic shaft is marked by a thin green line. In the *ko* neurons expressing synGAP, the percent of protrusions containing PSD-95 puncta is reduced toward that of *wt* neurons. In contrast, the size and brightness of PSD-95 puncta still resemble that of *ko* neurons. (C) Immunostaining for synGAP in the dendritic segments shown in (A). Dendritic shaft is marked as in (B). Antibodies against synGAP recognize recombinant synGAP^{wt}. The expression of synGAP^{wt} in dendrites of infected *ko* neurons was similar to that of endogenous synGAP in *wt* neurons. (D) Overlay of GFP (green), PSD-95 (red) and synGAP (blue) images.

Interestingly, the transient expression of synGAP^{wt} did not reverse the effect of the *ko* mutation on the size and brightness of immunostained PSD-95 puncta (Fig. 3.10, 3.11H). This result suggests that formation of PSD-95 clusters occurred before significant expression of synGAP^{wt} began on day 9. Functional protein clusters exist in dynamic equilibrium with monomers; therefore, this result also suggests that the rate of exchange between large clusters of PSD-95 and monomers or small clusters must be quite slow. Thus, 18 hours is not long enough for newly introduced synGAP to shift the equilibrium back toward the smaller clusters observed in *wt* neurons on day 10.

3.8 Role of the GAP domain and the t-T/SXV motif in spine maturation

To determine whether the Ras GTPase-activating activity of synGAP or its ability to bind to the PDZ domains of PSD-95 are important for spine maturation, we infected *ko* neurons with Sindbis viruses engineered to express GFP and synGAP with mutations in either of these two domains. The GAP domain was mutated at three critical residues as described in Section 2.7 (GAP^{mut}). Mutation of homologous residues in p120 RasGAP dramatically reduces its GAP catalytic rate and its affinity for Ras [Ahmadian et al., 1997, Skinner et al., 1991]. The five carboxyl terminal residues were truncated to delete the t-T/SXV domain of synGAP as described in Section 2.7 (ΔSXV). Hippocampal neurons were infected at 9 DIV with the viruses expressing each of the mutant synGAPs and their effects were compared to those of synGAP^{wt} expressed in *ko* neurons (*ko* + synGAP^{wt}; Fig. 3.11).

The ΔSXV mutation makes synGAP unable to rescue three of the spine phenotypes observed in *ko* neurons at 10 DIV. Expression of ΔSXV in *ko* neurons does not alter the width of protrusions at 10 DIV (Fig. 3.11A and F) and does not decrease the proportion of protrusions that contain PSD-95 (Fig. 3.11B and G). We also found that expression of synGAP^{wt} in *ko* neurons reduces the proportion of total PSD-95

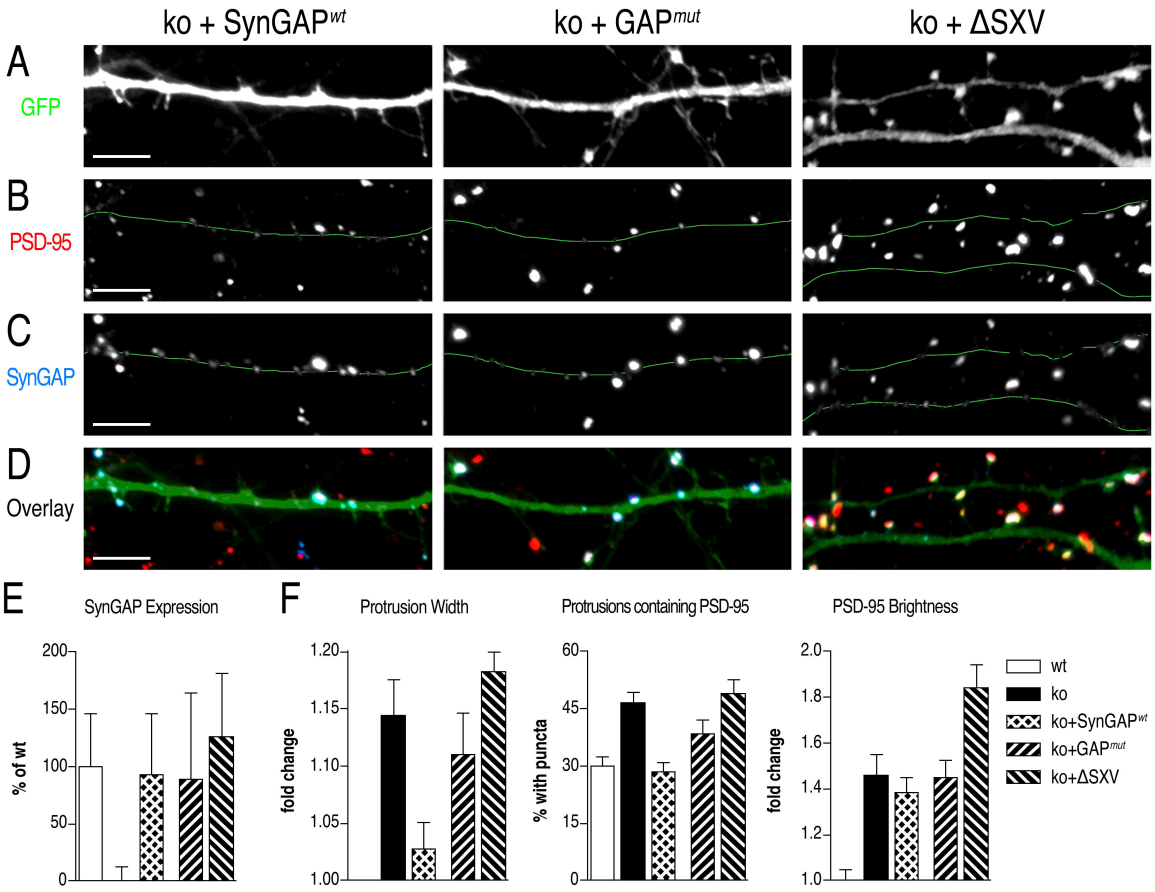

Figure 3.11: **Both the GAP domain and the PDZ domain-binding motif of synGAP are necessary to rescue precocious spine maturation in hippocampal neurons at 10 DIV.** (A) Representative images of dendritic segments from *ko* neurons expressing GFP, and either synGAP^{wt}, synGAP with a mutated GAP domain (GAP^{mut}), or synGAP with a deletion of the t-T/SXV domain (ΔSXV). Expression of synGAP^{wt}, but not GAP^{mut} or ΔSXV in *ko* neurons shifts the appearance of dendritic protrusions back toward that of *wt*. (B) Immunostaining for PSD-95 in the dendritic segments shown in (A). The location of the dendritic shaft is marked by a thin green line. The percent of protrusions containing PSD-95 was shifted back toward that of *wt* after expression of synGAP^{wt}, but not after expression of ΔSXV. In contrast, expression of GAP^{mut} caused a slight shift of the percent of protrusions containing PSD-95 back toward *wt* that was not statistically significant (see G). Finally, the brightness of PSD-95 puncta was not shifted at all toward *wt* by expression of synGAP^{wt}, GAP^{mut}, or ΔSXV. (C) Immunostaining for synGAP in the dendritic segments shown in (A). The dendritic shaft is marked as in (B). The synGAP antibody recognizes recombinant synGAP^{wt}, GAP^{mut} and ΔSXV. The expression of recombinant synGAP in dendrites of infected *ko* neurons was similar to that of endogenous synGAP in *wt* neurons. Also note that the t-T/SXV motif of synGAP is not necessary to target synGAP to dendritic protrusions. (D) Overlay of GFP (green), PSD-95 (red) and synGAP (blue) images.

Figure 3.11: Continued.
(E) Quantification of fluorescent staining for synGAP in dendrites measured as described in Section 2.9.4. SynGAP brightness (% of *wt*; mean ± sd): *wt*, 100.0 ± 45.8; *ko*, 0.0 ± 12.3; *ko* + synGAP^{wt}, 93.0 ± 53.1; *ko* + GAP^{mut}, 90.0 ± 75.2; *ko* + ΔSXV, 126.0 ± 55.2. Measurements were made of dendrites from 31 *wt* neurons prepared from 5 *wt* embryos, and of dendrites of 29 *ko* neurons, 32 *ko* + synGAP^{wt} neurons, 22 *ko* + GAP^{mut} neurons, and 17 *ko* + ΔSXV neurons from 4 *ko* embryos. Note that expression levels of synGAP in individual neurons are highly variable. (F) Quantification of width of protrusions. Measurements were made as described in Section 2.9.4. Protrusion widths (normalized to *wt*; mean ± sem): *wt*, 1.000 ± 0.000; *ko*, 1.144 ± 0.085; *ko* + synGAP^{wt}, 1.027 ± 0.023; *ko* + GAP^{mut}, 1.110 ± 0.036; *ko* + ΔSXV, 1.182 ± 0.017. Measurements were made of 3,608 protrusions from 31 *wt* neurons prepared from 5 *wt* embryos, and 3,434 protrusions from 29 textitko neurons, 3,486 protrusions from 32 *ko* + synGAP^{wt} neurons, 2,068 protrusions from 22 *ko* + GAP^{mut} neurons and 1,421 protrusions from 17 *ko* + ΔSXV neurons prepared from 4 *ko* embryos. The experiment was repeated at least 3 times for each viral construct (synGAP^{wt}, GAP^{mut} and ΔSXV) and similar results were obtained in each experiment. Therefore, the mean widths from all experiments were averaged. A P value of 0.0002 was obtained in a one-way ANOVA test, indicating a low probability that all of the means for each condition are the same. A Newman-Keuls post- test was performed to estimate the P values between each group. For *wt* vs. *ko*, $P < 0.01$; for *wt* vs. *ko* + GAP^{mut}, $P < 0.05$; for *wt* vs. *ko* + ΔSXV, $P < 0.01$; for *ko* vs. *ko* + synGAP^{wt}, $P < 0.05$; and for *ko* + synGAP^{wt} vs. *ko* + ΔSXV, $P < 0.01$. All other comparisons had $P > \tilde{0}.05$ and thus are considered not significantly different. The same P value estimates were obtained using the Tukey test, except that for *wt* vs. *ko* + GAP^{mut} which was $P > \tilde{0}.05$. (G) Quantification of percent of protrusions containing PSD-95. Measurements were made as described in Section 2.9.4. Percent of protrusions containing PSD-95 (mean ± sem): *wt*, 29.97 ± 2.38; *ko*, 46.51 ± 2.82; *ko* + synGAP^{wt}, 28.47 ± 2.50; *ko* + GAP^{mut}, 38.37 ± 3.55; *ko* + ΔSXV= 48.97 ± 3.75. Measurements were made of 2,530 PSD-95 puncta in dendrites of 31 *wt* neurons prepared from 5 *wt* embryos, and 2,023 PSD-95 puncta in dendrites of 29 *ko* neurons, 1,974 PSD-95 puncta in dendrites of 32 *ko* + synGAP^{wt} neurons, 2,973 PSD-95 puncta in dendrites of 22 *ko* + GAP^{mut} neurons and 2509 PSD-95 puncta in dendrites of 17 *ko* + ΔSXV neurons prepared from 4 *ko* embryos. A P value of less than 0.0001 was obtained in a one-way ANOVA test. A Newman-Keuls post-test was performed to estimate the P values between each group. For *wt* vs. *ko*, $P < 0.001$; for *ko* vs. *ko* + synGAP^{wt}, $P < 0.001$; for *wt* vs. *ko* + ΔSXV, $P < 0.01$; for *ko* + synGAP^{wt} vs *ko* + ΔSXV, $P < 0.01$. All other comparisons had $P > \tilde{0}.05$. The same P value estimates were obtained using the Tukey test. (H) Quantification of brightness of PSD-95 puncta. Brightness of fluorescent PSD-95 puncta (normalized to *wt*; mean ± sem): *wt*, 1.000 ± 0.046; *ko*, 1.461 ± 0.088; *ko* + synGAP^{wt}, 1.386 ± 0.064; *ko* + GAP^{mut}, 1.447 ± 0.077; *ko* + ΔSXV, 1.844 ± 0.097. Measurements were made on the same data set used in (G). A P value of less than 0.0001 was obtained in the one-way ANOVA test. A Newman-Keuls post-test was performed to estimate the P values between each group. For *wt* vs. *ko*, *ko* + synGAP^{wt}, *ko* + GAP^{mut}, or *ko* + ΔSXV, $P < 0.001$; for *ko* + ΔSXV vs. *ko* + synGAP^{wt}, $P < 0.001$; for *ko* + ΔSXV vs *ko*, or *ko* + GAP^{mut}, $P < 0.01$. All other comparisons had $P > \tilde{0}.05$. The same P value estimates were obtained using the Tukey test, except that for *ko* + ΔSXV vs *ko* + GAP^{mut} which was $P < 0.05$.

clusters that have moved into protrusions, whereas expression of ΔSXV does not. The proportion of PSD-95 clusters in protrusions increases 2.30 ± 0.15 fold in *ko* neurons compared to *wt* ($P < 0.001$; see also Fig. 3.5C). Expression of synGAP^{wt} in *ko* neurons reduces the proportion of clusters in protrusions to 1.50 ± 0.20 that of *wt* ($P > 0.05$, not statistically different from *wt*). In contrast, expression of ΔSXV in *ko* neurons has no effect on the proportion of clusters in protrusions (2.44 ± 0.27 fold of *wt* ; $P < 0.001$). Thus, the t-T/SXV domain is necessary for synGAP's role in retarding widening of spine heads and in movement of PSD-95 clusters into spines.

The effects of the GAP^{mut} mutation on these phenotypes is less dramatic. Expression of GAP^{mut} in *ko* neurons reduces the widths of their protrusions on 10 DIV, but the difference from *ko* neurons alone is not statistically significant (Fig. 3.11A and F). The GAP^{mut} shifts the mean percentage of spines containing PSD-95 to about halfway between *wt* and *ko* neurons; but the mean is not significantly different from either *wt* or *ko*, as indicated by ANOVA tests (Fig. 3.11B and G). The effect of GAP^{mut} in *ko* neurons does not differ from the effect of synGAP^{wt} on the proportion of total PSD-95 clusters in protrusions (1.49 ± 0.18 fold that of *wt*). Thus, the GAP domain may have a role in these phenotypes, but it appears to be a less crucial role than that of the t-T/SXV domain. It is important to keep in mind that GAP activity is reduced, but not abolished completely, by the mutations that we introduced into the GAP domain [Ahmadian et al., 1997, Skinner et al., 1991]. Therefore residual GAP activity could account for the relatively weak effects of these mutations on spine maturation. Nonetheless, the results indicate that both the t-T/SXV and the GAP domains are necessary for maximum rescue of precocious spine maturation; however, the mechanisms by which they act are likely to be at least partially distinct.

Neither expression of synGAP^{wt} nor of GAP^{mut} reverses the larger size of PSD-95 clusters (Fig. 3.11B and H, note that brightness correlates with area in these images). Expression of t-T/SXV actually increases their average size further. This result adds support to the conclusion that the GAP domain and the t-T/SXV domains affect different mechanisms during spine maturation.

Chapter 4

Discussion

4.1 Effects of synGAP deletion on spine maturation and structure

Other labs have reported that overexpression of certain PSD proteins can increase the size of spine heads [El-Husseini et al., 2000, Pak et al., 2001, Sala et al., 2001]. In contrast, we find that elimination of expression of synGAP leads to precocious synapse formation in developing neurons in culture and an increase in the size of spine heads in mature neurons. This result suggests that synGAP normally slows synapse formation and decreases the size of spine heads, perhaps reflecting its regulatory function.

We have shown that neurons with a deletion of the synGAP gene grow well in culture, and that spines and glutamatergic synapses form earlier in *ko* neurons than in *wt* neurons cultured under the same conditions. This effect is most apparent at 10 DIV when most of the dendritic protrusions in *wt* neurons still have the appearance of fine filopodia; but, in *ko* neurons, a larger proportion have the appearance of mature spines with wide heads. Immunolabeled clusters of PSD-95, AMPA and NMDA receptors are larger in *ko* neurons than in *wt* neurons and many more of the clusters are located in protrusions that resemble spines, rather than in the dendritic shaft. In *ko* neurons, more spines are associated with presynaptic terminals containing synapsin and more of them contain both AMPA and NMDA receptors, rather than NMDA receptors alone. Finally, the frequency and amplitude of mEPSCs are higher in *ko*

neurons compared to *wt* neurons at 10 DIV. All of these observations demonstrate that spine and synapse formation is accelerated in cultured neurons in the absence of synGAP. The effect of loss of synGAP on the appearance of spines is not confined to developmental stages. In mature neurons at 21 DIV, spines and their associated clusters of PSD-95 are still larger in *ko* neurons than in *wt*.

Some of the effects on spine structure at 10 DIV can be reversed by transient expression of *wt* synGAP in *ko* neurons at 9 DIV. Eighteen hours after infection with a virus expressing synGAP, the level of synGAP in dendrites has returned to that of *wt*, and the population of protrusions has shifted back toward those resembling thin filopodia rather than mature spines. Thus, the timing of spine maturation is directly affected by the absence or presence of synGAP on days 9 and 10, rather than indirectly affected by a change in the neurons caused by the absence of synGAP before day 9. This result means that the processes governing spine maturation in young neurons are dynamic and can be shifted rapidly toward more or fewer mature spines.

4.2 Mechanisms of spine maturation that are altered by synGAP deletion

Maximum reversal of precocious spine maturation by synGAP requires both a fully active GAP domain and a t-T/SXV domain. The inability of synGAP with mutations in these domains to fully rescue the *ko* phenotype means that both regulation of Ras inactivation by synGAP and its precise localization in the NMDA receptor signaling complex are important for controlling spine maturation. However, the effects of mutations in these two domains on the reversal by synGAP are different, suggesting that they influence spine maturation by at least partially different mechanisms (Fig. 4.1).

The results suggest that synGAP affects at least three distinct processes involved in spine formation; clustering of PSD proteins, widening of the spine head, and movement of PSD proteins into the spine head. The absence of synGAP leads to formation

of larger clusters of PSD-95, AMPA receptors, and NMDA receptors. This effect at day 10 DIV is not reversible by transient expression of synGAP beginning at 9 DIV. Thus, formation of the clusters likely begins earlier than day 9 *in vitro*, and the clusters are stable enough that they do not decrease in size in response to expression of synGAP for 24 hours. Transient expression of the ΔSXV mutant dramatically increases the size of PSD-95 clusters. As yet, we have no mechanistic explanation for this apparent dominant negative effect (see Section 6.1).

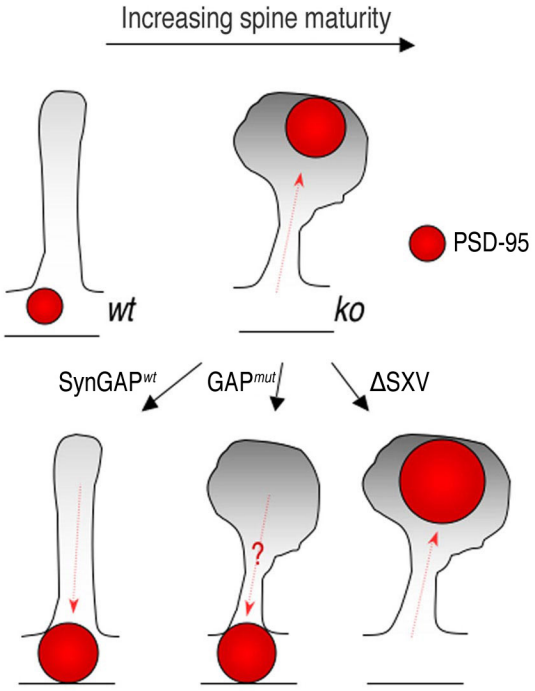

Figure 4.1: **Effects of synGAP on spine maturation.** (*Top*) At 10 DIV, the majority of protrusions in *wt* neurons resemble filopodia that lack PSD-95 whereas in *ko* neurons, many more protrusions resemble spines with PSD-95 in them. (*Bottom*) Reintroduction of *wt* synGAP into *ko* neurons at the 9^{th} DIV (expressed for 18 h thereafter) was sufficient to almost completely rescue the *ko* precocious spine maturation. However, reintroduction of the GAP domain mutant (GAP^{mut}) had no effect on the spine morphology and slightly retarded the movement of PSD-95 into spines. Reintroduction of the ΔSXV exacerbated the *ko* phenotype, and most notably increased PSD-95 brightness. The '?' in the spine depicting reintroduction of the GAP^{mut} indicates that the head-bearing spines that lacked PSD-95 were relatively rare. Nevertheless, retardation of PSD-95 movement into spines by reintroduction of GAP^{mut} was significant.

The absence of synGAP also leads to wider spine heads in *ko* neurons beginning at 10 DIV and continuing until at least 21 DIV. This effect at 10 DIV is reversed by transient expression of wtSynGAP at 9 DIV; however, mutation of the t-T/SXV

domain blocks the reversal and mutation of the GAP domain reduces it. Thus, both domains participate in synGAP's role in retarding widening of spine heads and prolonging the period of filopodial extension. The GAP domain is expected to increase the rate of inactivation of GTP-bound Ras. In the absence of synGAP it is possible that regulation of Ras in the postsynaptic compartment is disrupted. In many cells, Ras activation can lead to activation of the Rho family of GTP-binding proteins and to activation of PI3 kinase, both of which regulate the actin cytoskeleton [Hall, 1998, Kodaki et al., 1994, Rodriguez-Viciana et al., 1994, 1997]. Thus, the importance of the GAP domain for broadening of the spine head may be explained by its putative effects on the cytoskeleton (see Section 6.2).

It is less clear how the t-T/SXV domain might influence spine width. One clue comes from the effect of the ΔSXV mutation on movement of PSD-95 clusters into spines. The absence of synGAP in *ko* neurons accelerates movement of PSD-95 into spine heads; reintroduction of synGAP or of the GAP^{mut} into *ko* neurons at 9 DIV reverses this effect. In contrast, reintroduction of the ΔSXV mutant produces no reversal of the effect. One potential explanation of this result is that the ability of synGAP to bind to the PDZ domains of PSD-95 allows synGAP to compete for binding with another protein that functions to move PSD-95 clusters into the spine. In the absence of the t-T/SXV domain of synGAP, we predict that more of this hypothetical protein binds to PSD-95 and its movement into spines is accelerated.

This hypothesis is related to the more general hypothesis that altering the ratio among PSD proteins in dendrites can shift the equilibrium of spine size and/or size of protein clusters. This general hypothesis is supported by studies showing that overexpression of PSD-95 [El-Husseini et al., 2000], Shank [Sala et al., 2001], and SPAR [Pak et al., 2001] in cultured neurons increases the size of spine heads and of clusters of PSD proteins. We hypothesize that synGAP normally competes for binding to PSD-95 with proteins that increase the size of PSD- 95 clusters. This competition limits the size of clusters of PSD-95 and its associated proteins. When the competition is removed, the sizes of clusters increase. Potential synGAP competitors for binding to PDZ3 of PSD-95 are Kalirin [Penzes et al., 2001, 2003] and Stargazin [Schnell

et al., 2002] (see Section 6.1).

Zhu et al. [2002] recently investigated the effect of Ras activation on AMPA and NMDA receptor currents in cultured rat hippocampal slices (see Section 1.3.2). When Ras activity was transiently increased, AMPA but not NMDA receptor currents increased. Deletion of synGAP would be expected to produce a higher level of basal Ras activation at synapses. Thus, the model of Zhu et al. would predict the increase in AMPA receptor currents that we observe in cultured *ko* neurons.

In a separate study by Zhu, AMPAR currents were measured in hippocampal slices after NMDAR activity was chronically blocked from one to twelve days in culture [Zhu et al., 2002]. Interestingly, they observed a decrease in AMPAR-to-NMDAR current ratio after the first day that persisted until the eighth day. From the eighth day on, this ratio was indistinguishable from that in control slices, possibly due to homeostatic mechanisms [Rao and Craig, 1997, Turrigiano and Nelson, 2004]. We also observe an increase in the size and number of NMDA receptor and PSD-95 clusters at spines in synGAP *ko* neurons. Thus, it is possible that these changes result from a homeostatic response to the absence of synGAP, increased Ras activity and increased AMPAR currents.

In addition to the GAP and t-T/SXV domains, synGAP has other domains that may contribute to its functions. SynGAP and its related family member, p120 rasGAP, have a PH domain followed by a C2 domain located near the GAP domain. The PH domain of p120 RasGAP participates in regulation of its GAP activity [Drugan et al., 2000]; thus, the PH domain of synGAP may also be an important functional determinant. We have not yet explored the role of these additional domains in control of spine maturation (see Section 6.3).

4.3 Other synGAP *knockout* mutations

Two other laboratories have made deletion mutations of synGAP. One mutation deletes parts of the gene encoding the C2 and GAP domain [Komiyama et al., 2002]. Adult mice heterozygous for this mutation have abnormal long term potentiation.

The other mutation removes exons 7 and 8 which encode portions of the PH and C2 domains [Kim et al., 2003]. A low level ($\sim$2 % of *wt*) of synGAP splice variants containing a GAP domain is still expressed in these mice. They begin to weaken at P3 and die at P5 [Kim et al., 2003]; whereas mice homozygous for our deletion of exons 4 through 9 die by P2. The small amount of synGAP expression in the exon 7 and 8 deletion mutant may account for this difference. Kim et al. (2003) reported that cultured cortical neurons homozygous for the exon 7 and 8 deletion had 32 % more AMPA receptor clusters at 18-20 DIV than *wt* neurons, and about 20 % fewer 'silent' synapses that contain only NMDA receptors and no AMPA receptors. This observation may reflect the same alterations in regulation of spine maturation that we have described.

The findings presented here set the stage for a more detailed mechanistic analysis of the roles of Ras, PSD-95, and of various domains of synGAP in regulating spine maturation and the size of the PSD.

Chapter 5

Conclusions

We generated mice with a deletion in the synGAP gene to study the functions of synGAP and to enable identification of downstream pathways that are deregulated in its absence. As also shown by other groups [Kim et al., 2003, Komiyama et al., 2002], we find that mice with the homozygous synGAP deletion (*knockout*) die shortly after birth; however, neurons from *knockout* embryos can be maintained in culture. Here we report that spine maturation and synapse formation are altered in cultured *knockout* neurons. Spines and synapses form earlier in *knockout* neurons than in *wild-type* neurons, and spines ultimately become larger. Clusters of the PSD proteins PSD-95, NR1 and GluR1 are larger and brighter, and appear in spines earlier in *knockout* neurons. We conclude that the absence of synGAP results in accelerated synapse formation and larger spines in cultured neurons.

The altered spine development can be rescued by expression of *wild-type* synGAP in the *knockout* neurons. However, mutation of the GAP domain or removal of the t-T/SXV domain that associates with PSD-95 renders synGAP unable to rescue the *knockout* phenotype. The GAP-mutant synGAP slightly alleviates the *knockout* phenotype; however, it has no effect on spine morphology and only a subtle effect on the movement of PSD-95 into spines in *knockout* neurons. On the other hand, t-T/SXV-deleted synGAP, whose targeting to dendritic spines was unaffected, tends to exacerbate the *knockout* phenotype, and most notably increases PSD-95 brightness. Our results indicate that both GAP activity and interaction of synGAP with PSD-

95 play a role in determining the timing of spine maturation and the size of spines, probably involving different mechanisms.

We hypothesize that the GAP domain of synGAP regulates actin filament polymerization through regulation of Ras signaling pathways. Increased polymerization of actin filaments leads to increased spine size and head width associated with spine maturation. In the other hand, we hypothesize that the t-T/SXV motif of synGAP limits recruitment of PSD-95 to the PSD and/or PSD-95 multimerization. Increased recruitment of PSD-95 to the PSD or multimerization of PSD-95 at the PSD might trigger maturation of spines. Evidence for these hypotheses would elucidate two independent mechanisms by which spines mature, and would place synGAP as a link between them.

Chapter 6

Future Directions

The results presented in Chapter 3 indicate that synGAP regulates the timing of spine maturation and the size of mature spines. Taking advantage of the techniques used in this study, I will propose a few experiments that will further our understanding of the function of synGAP and the precise mechanism(s) by which synGAP regulates spine maturation. Specifically, I am interested in determining whether down-regulation of Ras by the GAP activity of synGAP is the critical means by which synGAP regulates spine formation. Indeed, the GAP domain of synGAP has received more attention than its other domains, and GAP activity is thought to be central to the protein's function. However, the data presented here indicates that the t-T/SXV motif of synGAP is also crucial for its role in synapse formation. I propose that the t-T/SXV motif of synGAP has a novel function independent of GAP activity; and will determine whether the t-T/SXV motif of synGAP regulates PSD-95 recruitment to the PSD, and/or PSD-95 multimerization. Also, I suspect that the PH and C2 domains of synGAP are involved in targeting synGAP to dendritic spines; nevertheless, these domains may also play roles in the regulation of synapse formation.

Although the results presented here indicate that synGAP has a major role in synapse formation, it is possible that synGAP is also involved in other cellular phenomena. Indeed, Irene Knuesel (a postdoctoral fellow in the Kennedy lab), found that synGAP is also involved in regulation of apoptotic cell death, another extremely complex cellular phenomenon. This indicates that synGAP, one of the most abundant proteins in the postsynaptic density, has many functions and is a critical protein for

neuronal physiology. Determining the mechanism by which synGAP regulates spine formation will at least serve to understand how different domains of synGAP can orchestrate the regulation of a complex neuronal process.

6.1 Role of the t-T/SXV motif of synGAP in regulating PSD-95 clustering

PSD-95 multimerization is highly regulated and can occur through various mechanisms [McGee et al., 2001, Hsueh et al., 1997, Morabito et al., 2004]. Increased PSD-95 clustering has been shown to accelerate spine maturation [El-Husseini et al., 2000]. In the absence of synGAP, clusters of immunostained PSD-95 are larger and brighter (Fig. 3.4). Furthermore, this increase in PSD-95 clustering is slightly exacerbated when the ΔSXV mutant is introduced into *ko* neurons (Fig. 3.11). These results suggest that synGAP might regulate PSD-95 clustering through its t-T/SXV motif. I will address two hypotheses by which the t-T/SXV motif of synGAP could affect PSD-95 clustering:

1. SynGAP binding to PSD-95 via its t-T/SXV motif down-regulates PSD-95 multimerization. This would explain why the absence of synGAP results in increased clustering of PSD-95. We can address this by transfecting cells with FLAG-tagged PSD-95 and Myc-tagged PSD-95 in the presence or absence of synGAP. By Myc-tag 'pull-down' of the cell extract and subsequent FLAG-tag immunoblotting, we can measure the amount of PSD-95 multimerization in the presence or absence of synGAP.

2. The t-T/SXV motif of synGAP ensures the specific localization of its GAP activity. Without its t-T/SXV motif, synGAP docking to the PSD might be perturbed. This could result in mislocated GAP activity and deregulation of signaling pathways, leading to increased PSD-95 clustering. This can be tested by introducing a mutant version of synGAP lacking both GAP activity and the

t-T/SXV motif (GAP^{mut}/ΔSXV) into *ko* neurons and determining whether the exacerbated effects on PSD-95 puncta caused by the ΔSXV are now abolished.

In addition to increasing PSD-95 clustering, absence of synGAP also accelerates the timing of PSD-95 movement from the dendritic shaft into spines (Fig. 3.5). Moreover, this alteration was corrected by either $synGAP^{wt}$ or GAP^{mut}, but not the ΔSXV mutant. This led us to hypothesize that the t-T/SXV motif of synGAP can hold PSD-95, and its bound proteins, from moving into spines (see Section 4.2). The pause in the movement of the PSD-95 complex into spines can serve as a checkpoint in the transition from filopodia to spine. Upon another signal (synaptic activity, polymerization of the actin cytoskeleton, or binding of another protein/s), this complex can then move into spines. We are currently addressing this hypothesis by screening PSD-95 interacting proteins for upregulation in the PSD of synGAP *heterozygote* mice.

6.2 Role of Ras in spine maturation

In some cell types, Ras has been shown to mediate changes in the actin cytoskeleton through activation of Rac [Innocenti et al., 1999, Kodaki et al., 1994, Krapivinsky et al., 2003, Nimnual and Bar-Sagi, 2002, Ridley et al., 1992], and active Rac leads to 'spinogenesis' in neurons [Tashiro et al., 2000, Bonhoeffer and Yuste, 2002]. Studies have shown that Ras activity increases filopodial growth and complexity of dendritic morphology [Wu et al., 2001, Alpar et al., 2003].

In the absence of synGAP it is possible that regulation of Ras in the postsynaptic compartment is disrupted [Oh et al., 2004]. This is supported by preliminary results that show increased basal levels of phosphorylated ERK in cultured *ko* neurons (Fig. 6.1). Here, we showed that absence of synGAP leads to increased head width of spines (Fig. 3.3). Furthermore, we showed that introducing GAP-mutant synGAP (GAP^{mut}) into *ko* neurons is incapable of rescuing the head width of spines (Fig. 3.11), suggesting that synGAP's GAP activity influences the actin cytoskeleton of spines.

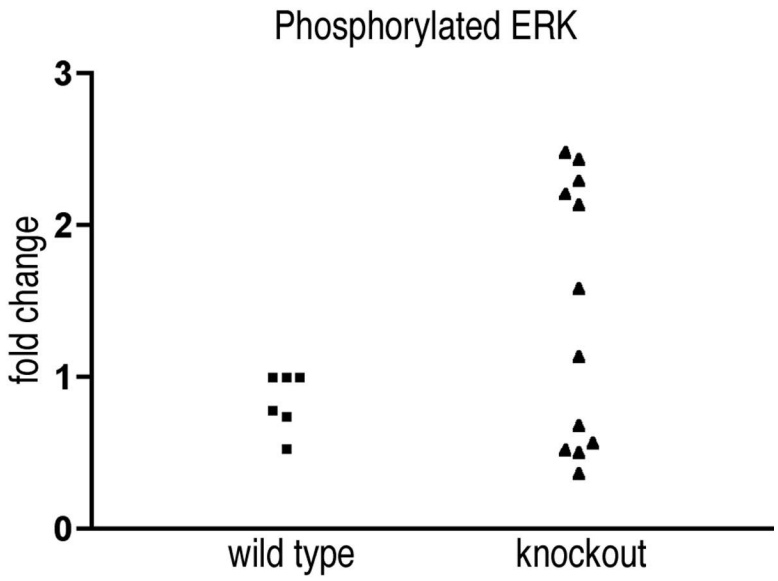

Figure 6.1: **Basal levels of phosphorylated ERK 1/2 in neuronal cultures**. Extracts from *wt* and *ko* cultured neurons were collected and levels of phosphorylated ERK (P-ERK) were analyzed by immunoblotting (see Section 2.6). Scanned blots were quantified using Image Quant software (Molecular Dynamics, Inc.). Data pooled from 3 experiments; individual experiments were normalized to their highest intensity *wt* band. P-ERK levels are slightly higher in *ko* neurons (P= 0.058, Student's t-test).

We hypothesize that increased Ras activity due to the absence of synGAP leads to increased polymerization of the spine actin cytoskeleton. To test this hypothesis, we will express dominant negative Ras (RasN17) in synGAP *ko* neurons [Feig, 1999]. To accomplish this, we will infect 9 DIV synGAP *ko* neurons with a Sindbis virus engineered to express RasN17 fused to GFP [Zhu et al., 2002](Sindbis/RasN17-GFP DNA was a gift of Julius Zhu and Roberto Malinow). Eighteen hours after infection, we will stain infected *ko* neurons for both actin (spine marker) and PSD-95, and analyze obtained images as described in Section 2.9.

From this experiment, we predict that a decrease in Ras activity after several hours of RasN17 expression [Zhu et al., 2002] will result in a reorganization of the actin cytoskeleton of spines as indicated by a reduction in the head width of spines. Taking in consideration that synGAP binding to PSD-95 is also necessary for adequate spine maturation (Section 3.8), reducing Ras activity alone should only result in a partial rescue of the *ko* phenotype.

Full rescue of the *ko* phenotype by RasN17 might indicate that synGAP binding to PSD-95 serves to localize its GAP activity. This possibility is considered in Section 6.1.

6.3 Role of the N-terminus of synGAP

A surprising finding of this study was that the t-T/SXV motif is not required for targeting synGAP to dendritic spines (see Section 3.8). Intrigued by this finding, we wish to identify the regions of synGAP that regulate its targeting to dendritic spines. Because PH and C2 domains have been implicated in phospholipid binding and membrane association [Lemmon et al., 2002, DiNitto et al., 2003], we hypothesize that the PH and C2 domains of synGAP are involved in its targeting to spines. To address this, the following mutations were created: a PH domain deletion, and deletion of both the PH and C2 domains. By incorporating these synGAP mutants into the Sindbis virus used in this study we will analyze their localization relative to *wt* synGAP as described in Section 3.8.

The PH domain of p120 RasGAP participates in regulation of its GAP activity [Drugan et al., 2000], and PH domain-mediated membrane recruitment of proteins contributes to regulated actin assembly and cell polarization [Lemmon et al., 2002]. Also, Ca^{2+} can regulate membrane recruitment of certain proteins through their C2 domains [Stevens and Sullivan, 2003]. In the case that the PH- and PH/C2-deleted synGAP targets to dendritic spines, we will determine their effect on spine maturation as in Section 3.8.

6.4 Protein expression in synGAP *ko* neurons

We showed that immunostained puncta for PSD-95, NR1 and GluR1 are larger and brighter in 10 DIV *ko* neurons (Section 3.4). This observation suggests that synthesis or degradation of these proteins might be altered in *ko* neurons. To test this, extracts from 7, 10 and 21 DIV cultures will be collected and the levels of PSD-95, NR1,

GluR1 and other proteins will be analyzed by Western blot.

Because the increase in size and brightness of PSD-95, NR1 and GluR1 proteins was less than 2 fold when analyzed by immunostaining (Fig. 3.4), it is possible that no differences will be observed by Western blot analysis. In fact, Irene Knuesel did not detect differences in the levels of PSD-95, NR1 and GluR1 from P1 brain homogenates by Western blot analysis (Fig. 6.2). Nevertheless, the synthesis of many synaptic proteins in the hippocampus of *wt* mice is minimal at P1, and increases gradually thereafter (Appendix A). Therefore, levels of synaptic proteins in the P1 hippocampus might not reflect those in 7 or 10 DIV hippocampal cultures.

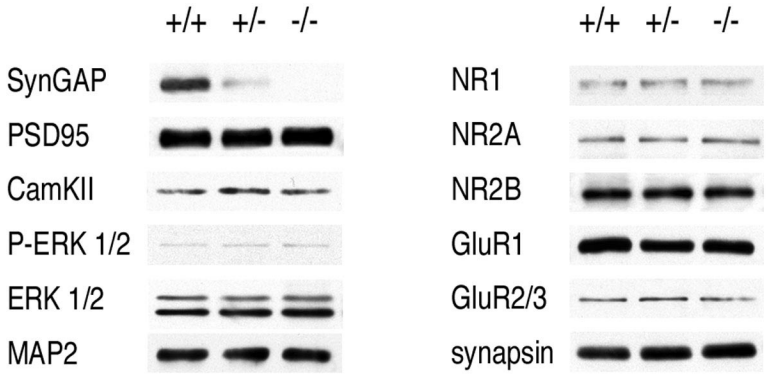

Figure 6.2: **Western blot analysis of P1 brain homogenates.** Postnatal day 1 mouse brains were homogenized and protein levels were analyzed by Western blot. No differences in the levels of tested proteins were observed between *wt* and *ko* mice.

Despite Irene Knuesel's findings (Fig. 6.2), it is essential to determine whether in 10 DIV culture extracts there is no change, or a small increase in the expression of these proteins. The former case supports a change in the distribution of these proteins (Fig. 3.5), whereas the latter would also imply up-regulation in protein synthesis or down-regulation of protein degradation. This experiment will also pave the way to finding other proteins working in signal-transduction pathways that involve synGAP.

Bibliography

M. R. Ahmadian, P. Stege, K. Scheffzek, and A. Wittinghofer. Confirmation of the arginine-finger hypothesis for the GAP-stimulated GTP-hydrolysis reaction of Ras. *Nat Struct Biol*, 4(9):686–689, Sep 1997.

M. Alonso, J. H. Medina, and L. Pozzo-Miller. ERK1/2 activation is necessary for BDNF to increase dendritic spine density in hippocampal CA1 pyramidal neurons. *Learn Mem*, 11(2):172–178, Mar 2004.

A. Alpar, K. Palm, A. Schierwagen, T. Arendt, and U. Gartner. Expression of constitutively active p21H-rasval12 in postmitotic pyramidal neurons results in increased dendritic size and complexity. *J Comp Neurol*, 467(1):119–33, Dec 2003.

C. H. Bailey and E. R. Kandel. Structural changes accompanying memory storage. *Annu Rev Physiol*, 55:397–426, 1993.

G. Banker, L. Churchill, and C. W. Cotman. Proteins of the postsynaptic density. *J Cell Biol*, 63(2 Pt 1):456–65, Nov 1974.

F. Blomberg, R. S. Cohen, and P. Siekevitz. The structure of postsynaptic densities isolated from dog cerebral cortex. II. Characterization and arrangement of some of the major proteins within the structure. *J Cell Biol*, 74(1):204–25, Jul 1977.

T. Bonhoeffer and R. Yuste. Spine motility. Phenomenology, mechanisms, and function. *Neuron*, 35(6):1019–27, Sep 2002.

G. J. Brewer, J. R. Torricelli, E. K. Evege, and P. J. Price. Optimized survival of hippocampal neurons in B27-supplemented Neurobasal, a new serum-free medium combination. *J Neurosci Res*, 35(5):567–76, Aug 1993.

H. J. Chen, M. Rojas-Soto, A. Oguni, and M. B. Kennedy. A synaptic Ras-GTPase activating protein (p135 SynGAP) inhibited by CaM kinase II. *Neuron*, 20(5): 895–904, May 1998.

K. O. Cho, C. A. Hunt, and M. B. Kennedy. The rat brain postsynaptic density fraction contains a homolog of the Drosophila discs-large tumor suppressor protein. *Neuron*, 9(5):929–42, Nov 1992.

R. S. Cohen, F. Blomberg, K. Berzins, and P. Siekevitz. The structure of postsynaptic densities isolated from dog cerebral cortex. I. Overall morphology and protein composition. *J Cell Biol*, 74(1):181–203, Jul 1977.

M. Constantine-Paton, H. T. Cline, and E. Debski. Patterned activity, synaptic convergence, and the NMDA receptor in developing visual pathways. *Annu Rev Neurosci*, 13:129–54, 1990.

A. Contractor and S. F. Heinemann. Glutamate receptor trafficking in synaptic plasticity. *Sci STKE*, 2002(156):RE14, Oct 2002.

C. W. Cotman, G. Banker, L. Churchill, and D. Taylor. Isolation of postsynaptic densities from rat brain. *J Cell Biol*, 63(2 Pt 1):441–55, Nov 1974.

J. P. DiNitto, T. C. Cronin, and D. G. Lambright. Membrane recognition and targeting by lipid-binding domains. *Sci STKE*, 2003(213):re16, Dec 2003.

J. K. Drugan, K. Rogers-Graham, T. Gilmer, S. Campbell, and G. J. Clark. The Ras/p120 GTPase-activating protein (GAP) interaction is regulated by the p120 GAP pleckstrin homology domain. *J Biol Chem*, 275(45):35021–35027, Nov 2000.

G. M. Durand, Y. Kovalchuk, and A. Konnerth. Long-term potentiation and functional synapse induction in developing hippocampus. *Nature*, 381(6577):71–75, May 1996.

F. A. Edwards. Dancing dendrites. *Nature*, 394(6689):129–30, Jul 1998.

M. D. Ehlers. Reinsertion or degradation of AMPA receptors determined by activity-dependent endocytic sorting. *Neuron*, 28(2):511–25, Nov 2000.

A. E. El-Husseini, E. Schnell, D. M. Chetkovich, R. A. Nicoll, and D. S. Bredt. PSD-95 involvement in maturation of excitatory synapses. *Science*, 290(5495):1364–1368, Nov 2000.

F. Engert and T. Bonhoeffer. Dendritic spine changes associated with hippocampal long-term synaptic plasticity. *Nature*, 399(6731):66–70, May 1999.

L. A. Feig. Tools of the trade: use of dominant-inhibitory mutants of Ras-family GTPases. *Nat Cell Biol*, 1(2):E25–7, Jun 1999.

J. C. Fiala, M. Feinberg, V. Popov, and K. M. Harris. Synaptogenesis via dendritic filopodia in developing hippocampal area CA1. *J Neurosci*, 18(21):8900–11, Nov 1998.

J. C. Fiala, J. Spacek, and K. M. Harris. Dendritic spine pathology: cause or consequence of neurological disorders? *Brain Res Brain Res Rev*, 39(1):29–54, Jun 2002.

E. Fifkova and R. J. Delay. Cytoplasmic actin in neuronal processes as a possible mediator of synaptic plasticity. *J Cell Biol*, 95(1):345–50, Oct 1982.

M. Fischer, S. Kaech, D. Knutti, and A. Matus. Rapid actin-based plasticity in dendritic spines. *Neuron*, 20(5):847–54, May 1998.

M. Fischer, S. Kaech, U. Wagner, H. Brinkhaus, and A. Matus. Glutamate receptors regulate actin-based plasticity in dendritic spines. *Nat Neurosci*, 3(9):887–94, Sep 2000.

E.G. Gray. Electron microscopy of synaptic contacts on dendritic spines of the cerebral cortex. *Nature*, (183):1592–1594, 1959.

J. Grutzendler, N. Kasthuri, and W. B. Gan. Long-term dendritic spine stability in the adult cortex. *Nature*, 420(6917):812–816, Dec 2002.

A. Hall. Rho GTPases and the actin cytoskeleton. *Science*, 279(5350):509–14, Jan 1998.

K. M. Harris, J. C. Fiala, and L. Ostroff. Structural changes at dendritic spine synapses during long-term potentiation. *Philos Trans R Soc Lond B Biol Sci*, 358 (1432):745–748, Apr 2003.

K. M. Harris and S. B. Kater. Dendritic spines: cellular specializations imparting both stability and flexibility to synaptic function. *Annu Rev Neurosci*, 17:341–71, 1994.

A. J. Heynen, E. M. Quinlan, D. C. Bae, and M. F. Bear. Bidirectional, activity-dependent regulation of glutamate receptors in the adult hippocampus in vivo. *Neuron*, 28(2):527–36, Nov 2000.

Y. P. Hsueh, E. Kim, and M. Sheng. Disulfide-linked head-to-head multimerization in the mechanism of ion channel clustering by PSD-95. *Neuron*, 18(5):803–14, May 1997.

H. Husi, M. A. Ward, J. S. Choudhary, W. P. Blackstock, and S. G. Grant. Proteomic analysis of NMDA receptor-adhesion protein signaling complexes. *Nat Neurosci*, 3 (7):661–669, Jul 2000.

M. Innocenti, R. Zippel, R. Brambilla, and E. Sturani. CDC25(Mm)/Ras-GRF1 regulates both Ras and Rac signaling pathways. *FEBS Lett*, 460(2):357–62, Oct 1999.

J. T. Isaac, R. A. Nicoll, and R. C. Malenka. Evidence for silent synapses: implications for the expression of LTP. *Neuron*, 15(2):427–34, Aug 1995.

Y. Ishikawa, H. Katoh, and M. Negishi. A role of Rnd1 GTPase in dendritic spine formation in hippocampal neurons. *J Neurosci*, 23(35):11065–72, Dec 2003.

M. B. Kennedy. The postsynaptic density at glutamatergic synapses. *Trends Neurosci*, 20(6):264–268, Jun 1997.

M. B. Kennedy. Signal transduction molecules at the glutamatergic postsynaptic membrane. *Brain Res Brain Res Rev*, 26(2-3):243–57, May 1998.

M. B. Kennedy. Signal-processing machines at the postsynaptic density. *Science*, 290 (5492):750–754, Oct 2000.

M. B. Kennedy, M. K. Bennett, and N. E. Erondu. Biochemical and immunochemical evidence that the "major postsynaptic density protein" is a subunit of a calmodulin-dependent protein kinase. *Proc Natl Acad Sci U S A*, 80(23):7357–61, Dec 1983.

J. H. Kim, H. K. Lee, K. Takamiya, and R. L. Huganir. The role of synaptic GTPase-activating protein in neuronal development and synaptic plasticity. *J Neurosci*, 23 (4):1119–24, Feb 2003.

J. H. Kim, D. Liao, L. F. Lau, and R. L. Huganir. SynGAP: a synaptic RasGAP that associates with the PSD-95/SAP90 protein family. *Neuron*, 20(4):683–91, Apr 1998.

G. W. Knott, C. Quairiaux, C. Genoud, and E. Welker. Formation of dendritic spines with GABAergic synapses induced by whisker stimulation in adult mice. *Neuron*, 34(2):265–73, Apr 2002.

T. Kodaki, R. Woscholski, B. Hallberg, P. Rodriguez-Viciana, J. Downward, and P. J. Parker. The activation of phosphatidylinositol 3-kinase by Ras. *Curr Biol*, 4(9): 798–806, Sep 1994.

N. H. Komiyama, A. M. Watabe, H. J. Carlisle, K. Porter, P. Charlesworth, J. Monti, D. J. Strathdee, C. M. O'Carroll, S. J. Martin, R. G. Morris, T. J. O'Dell, and S. G. Grant. SynGAP regulates ERK/MAPK signaling, synaptic plasticity, and learning in the complex with postsynaptic density 95 and NMDA receptor. *J Neurosci*, 22 (22):9721–32, Nov 2002.

B. Kramer, W. Kramer, and H. J. Fritz. Different base/base mismatches are corrected with different efficiencies by the methyl-directed DNA mismatch-repair system of E. coli. *Cell*, 38(3):879–87, Oct 1984.

G. Krapivinsky, L. Krapivinsky, Y. Manasian, A. Ivanov, R. Tyzio, C. Pellegrino, Y. Ben-Ari, D. E. Clapham, and I. Medina. The NMDA receptor is coupled to the ERK pathway by a direct interaction between NR2B and RasGRF1. *Neuron*, 40 (4):775–84, Nov 2003.

M. A. Lemmon, K. M. Ferguson, and C. S. Abrams. Pleckstrin homology domains and the cytoskeleton. *FEBS Lett*, 513(1):71–76, Feb 2002.

B. Lendvai, E. A. Stern, B. Chen, and K. Svoboda. Experience-dependent plasticity of dendritic spines in the developing rat barrel cortex in vivo. *Nature*, 404(6780): 876–81, Apr 2000.

W. Li, A. Okano, Q. B. Tian, K. Nakayama, T. Furihata, H. Nawa, and T. Suzuki. Characterization of a novel synGAP isoform, synGAP-beta. *J Biol Chem*, 276(24): 21417–24, Jun 2001.

D. Liao, N. A. Hessler, and R. Malinow. Activation of postsynaptically silent synapses during pairing-induced LTP in CA1 region of hippocampal slice. *Nature*, 375(6530): 400–404, Jun 1995.

D. Liao, X. Zhang, R. O'Brien, M. D. Ehlers, and R. L. Huganir. Regulation of morphological postsynaptic silent synapses in developing hippocampal neurons. *Nat Neurosci*, 2(1):37–43, Jan 1999.

J. W. Lin, W. Ju, K. Foster, S. H. Lee, G. Ahmadian, M. Wyszynski, Y. T. Wang, and M. Sheng. Distinct molecular mechanisms and divergent endocytotic pathways of AMPA receptor internalization. *Nat Neurosci*, 3(12):1282–90, Dec 2000.

L. Luo. Actin cytoskeleton regulation in neuronal morphogenesis and structural plasticity. *Annu Rev Cell Dev Biol*, 18:601–35, 2002.

X. M. Ma, J. Huang, Y. Wang, B. A. Eipper, and R. E. Mains. Kalirin, a multifunctional Rho guanine nucleotide exchange factor, is necessary for maintenance of hippocampal pyramidal neuron dendrites and dendritic spines. *J Neurosci*, 23(33): 10593–603, Nov 2003.

R. C. Malenka and R. A. Nicoll. NMDA-receptor-dependent synaptic plasticity: multiple forms and mechanisms. *Trends Neurosci*, 16(12):521–527, Dec 1993.

M. Maletic-Savatic, R. Malinow, and K. Svoboda. Rapid dendritic morphogenesis in CA1 hippocampal dendrites induced by synaptic activity. *Science*, 283(5409): 1923–1927, Mar 1999.

R. Malinow and R. C. Malenka. AMPA receptor trafficking and synaptic plasticity. *Annu Rev Neurosci*, 25:103–26, 2002.

G. S. Marrs, S. H. Green, and M. E. Dailey. Rapid formation and remodeling of postsynaptic densities in developing dendrites. *Nat Neurosci*, 4(10):1006–13, Oct 2001.

A. Matus. Actin-based plasticity in dendritic spines. *Science*, 290(5492):754–758, Oct 2000.

A. Matus. Moving molecules make synapses. *Nat Neurosci*, 4(10):967–968, Oct 2001.

A. Matus, M. Ackermann, G. Pehling, H. R. Byers, and K. Fujiwara. High actin concentrations in brain dendritic spines and postsynaptic densities. *Proc Natl Acad Sci U S A*, 79(23):7590–7594, Dec 1982.

A. K. McAllister, L. C. Katz, and D. C. Lo. Neurotrophin regulation of cortical dendritic growth requires activity. *Neuron*, 17(6):1057–64, Dec 1996.

A. W. McGee, S. R. Dakoji, O. Olsen, D. S. Bredt, W. A. Lim, and K. E. Prehoda. Structure of the SH3-guanylate kinase module from PSD-95 suggests a mechanism for regulated assembly of MAGUK scaffolding proteins. *Mol Cell*, 8(6):1291–301, Dec 2001.

Y. Meng, Y. Zhang, V. Tregoubov, C. Janus, L. Cruz, M. Jackson, W. Y. Lu, J. F. MacDonald, J. Y. Wang, D. L. Falls, and Z. Jia. Abnormal spine morphology and enhanced LTP in LIMK-1 knockout mice. *Neuron*, 35(1):121–33, Jul 2002.

M. A. Morabito, M. Sheng, and L. H. Tsai. Cyclin-dependent kinase 5 phosphorylates the N-terminal domain of the postsynaptic density protein PSD-95 in neurons. *J Neurosci*, 24(4):865–76, Jan 2004.

A. Y. Nakayama, M. B. Harms, and L. Luo. Small GTPases Rac and Rho in the maintenance of dendritic spines and branches in hippocampal pyramidal neurons. *J Neurosci*, 20(14):5329–38, Jul 2000.

A. Y. Nakayama and L. Luo. Intracellular signaling pathways that regulate dendritic spine morphogenesis. *Hippocampus*, 10(5):582–586, 2000.

A. Nimnual and D. Bar-Sagi. The two hats of SOS. *Sci STKE*, 2002(145):PE36, Aug 2002.

J. S. Oh, P. Manzerra, and M. B. Kennedy. Regulation of the neuron-specific Ras GTPase activating protein, synGAP, by Ca2+/calmodulin-dependent protein kinase II. *J Biol Chem*, Feb 2004.

S. Okabe, A. Miwa, and H. Okado. Spine formation and correlated assembly of presynaptic and postsynaptic molecules. *J Neurosci*, 21(16):6105–14, Aug 2001.

D. T. Pak, S. Yang, S. Rudolph-Correia, E. Kim, and M. Sheng. Regulation of dendritic spine morphology by SPAR, a PSD-95-associated RapGAP. *Neuron*, 31 (2):289–303, Aug 2001.

M. Passafaro, V. Piech, and M. Sheng. Subunit-specific temporal and spatial patterns of AMPA receptor exocytosis in hippocampal neurons. *Nat Neurosci*, 4(9):917–26, Sep 2001.

P. Penzes, A. Beeser, J. Chernoff, M. R. Schiller, B. A. Eipper, R. E. Mains, and R. L. Huganir. Rapid induction of dendritic spine morphogenesis by trans-synaptic ephrinB-EphB receptor activation of the Rho-GEF kalirin. *Neuron*, 37(2):263–74, Jan 2003.

P. Penzes, R. C. Johnson, R. Sattler, X. Zhang, R. L. Huganir, V. Kambampati, R. E. Mains, and B. A. Eipper. The neuronal Rho-GEF Kalirin-7 interacts with PDZ domain-containing proteins and regulates dendritic morphogenesis. *Neuron*, 29(1): 229–42, Jan 2001.

A. Peters and I.R. Kaiserman-Abramof. The small pyramidal neuron of the rat cerebral cortex. The perikaryon, dendrites and spines. *Am. J. Anat.*, (127):321–355, 1970.

R. S. Petralia, J. A. Esteban, Y. X. Wang, J. G. Partridge, H. M. Zhao, R. J. Wenthold, and R. Malinow. Selective acquisition of AMPA receptors over postnatal development suggests a molecular basis for silent synapses. *Nat Neurosci*, 2(1):31–36, Jan 1999.

S Ramon y Cajal. La Textura del Sistema Nervioso del Hombre y los Vertebrados. *(Madrid:Moya).*

S Ramon y Cajal. Estructura de los centros nerviosos de las aves. *Rev. Trim. Histol. Norm. Pat*, (1):1–10, 1888.

S Ramon y Cajal. Significación fisiológica de las expanciones protoplásmicas y nerviosas de la sustancia gris. *Revista de Ciencias Medicas de Barcelona*, (22): 23, 1891.

A. Rao and A. M. Craig. Activity regulates the synaptic localization of the NMDA receptor in hippocampal neurons. *Neuron*, 19(4):801–12, Oct 1997.

A. J. Ridley, H. F. Paterson, C. L. Johnston, D. Diekmann, and A. Hall. The small GTP-binding protein rac regulates growth factor-induced membrane ruffling. *Cell*, 70(3):401–10, Aug 1992.

P. Rodriguez-Viciana, P. H. Warne, R. Dhand, B. Vanhaesebroeck, I. Gout, M. J. Fry, M. D. Waterfield, and J. Downward. Phosphatidylinositol-3-OH kinase as a direct target of Ras. *Nature*, 370(6490):527–32, Aug 1994.

P. Rodriguez-Viciana, P. H. Warne, A. Khwaja, B. M. Marte, D. Pappin, P. Das, M. D. Waterfield, A. Ridley, and J. Downward. Role of phosphoinositide 3-OH kinase in cell transformation and control of the actin cytoskeleton by Ras. *Cell*, 89 (3):457–67, May 1997.

C. Sala, V. Piech, N. R. Wilson, M. Passafaro, G. Liu, and M. Sheng. Regulation of dendritic spine morphology and synaptic function by Shank and Homer. *Neuron*, 31(1):115–30, Jul 2001.

J. R. Sanes and J. W. Lichtman. Can molecules explain long-term potentiation? *Nat Neurosci*, 2(7):597–604, Jul 1999.

R. H. Scannevin and R. L. Huganir. Postsynaptic organization and regulation of excitatory synapses. *Nat Rev Neurosci*, 1(2):133–41, Nov 2000.

E. Schnell, M. Sizemore, S. Karimzadegan, L. Chen, D. S. Bredt, and R. A. Nicoll. Direct interactions between PSD-95 and stargazin control synaptic AMPA receptor number. *Proc Natl Acad Sci U S A*, 99(21):13902–13907, Oct 2002.

E. M. Schuman. mRNA trafficking and local protein synthesis at the synapse. *Neuron*, 23(4):645–648, Aug 1999.

M. Sheng. Molecular organization of the postsynaptic specialization. *Proc Natl Acad Sci U S A*, 98(13):7058–61, Jun 2001.

M. Sheng and E. Kim. The Shank family of scaffold proteins. *J Cell Sci*, 113 (Pt 11):1851–1856, Jun 2000.

M. Sheng and S. H. Lee. AMPA receptor trafficking and the control of synaptic transmission. *Cell*, 105(7):825–828, Jun 2001.

M. Sheng and C. Sala. PDZ domains and the organization of supramolecular complexes. *Annu Rev Neurosci*, 24:1–29, 2001.

S. Shi, Y. Hayashi, J. A. Esteban, and R. Malinow. Subunit-specific rules governing AMPA receptor trafficking to synapses in hippocampal pyramidal neurons. *Cell*, 105(3):331–43, May 2001.

S. H. Shi, Y. Hayashi, R. S. Petralia, S. H. Zaman, R. J. Wenthold, K. Svoboda, and R. Malinow. Rapid spine delivery and redistribution of AMPA receptors after synaptic NMDA receptor activation. *Science*, 284(5421):1811–1816, Jun 1999.

R. H. Skinner, S. Bradley, A. L. Brown, N. J. Johnson, S. Rhodes, D. K. Stammers, and P. N. Lowe. Use of the Glu-Glu-Phe C-terminal epitope for rapid purification of the catalytic domain of normal and mutant ras GTPase-activating proteins. *J Biol Chem*, 266(22):14163–14166, Aug 1991.

F. M. Smart and S. Halpain. Regulation of dendritic spine stability. *Hippocampus*, 10(5):542–54, 2000.

K. E. Sorra and K. M. Harris. Overview on the structure, composition, function, development, and plasticity of hippocampal dendritic spines. *Hippocampus*, 10(5): 501–11, 2000.

C. F. Stevens and J. M. Sullivan. The synaptotagmin C2A domain is part of the calcium sensor controlling fast synaptic transmission. *Neuron*, 39(2):299–308, Jul 2003.

A. Tashiro, A. Minden, and R. Yuste. Regulation of dendritic spine morphology by the rho family of small GTPases: antagonistic roles of Rac and Rho. *Cereb Cortex*, 10(10):927–38, Oct 2000.

J. T. Trachtenberg, B. E. Chen, G. W. Knott, G. Feng, J. R. Sanes, E. Welker, and K. Svoboda. Long-term in vivo imaging of experience-dependent synaptic plasticity in adult cortex. *Nature*, 420(6917):788–94, Dec 2002.

G. G. Turrigiano and S. B. Nelson. Homeostatic plasticity in the developing nervous system. *Nat Rev Neurosci*, 5(2):97–107, Feb 2004.

V. L. Tybulewicz, C. E. Crawford, P. K. Jackson, R. T. Bronson, and R. C. Mulligan. Neonatal lethality and lymphopenia in mice with a homozygous disruption of the c-abl proto-oncogene. *Cell*, 65(7):1153–63, Jun 1991.

R. S. Walikonis, O. N. Jensen, M. Mann, J. r. Provance D.W., J. A. Mercer, and M. B. Kennedy. Identification of proteins in the postsynaptic density fraction by mass spectrometry. *J Neurosci*, 20(11):4069–80, Jun 2000.

C. S. Woolley and B. S. McEwen. Estradiol regulates hippocampal dendritic spine density via an N-methyl-D-aspartate receptor-dependent mechanism. *J Neurosci*, 14(12):7680–7687, Dec 1994.

G. Y. Wu, K. Deisseroth, and R. W. Tsien. Spaced stimuli stabilize MAPK pathway activation and its effects on dendritic morphology. *Nat Neurosci*, 4(2):151–158, Feb 2001.

B. Xiao, J. C. Tu, and P. F. Worley. Homer: a link between neural activity and glutamate receptor function. *Curr Opin Neurobiol*, 10(3):370–374, Jun 2000.

R. Yuste and T. Bonhoeffer. Morphological changes in dendritic spines associated with long-term synaptic plasticity. *Annu Rev Neurosci*, 24:1071–89, 2001.

R. Yuste and T. Bonhoeffer. Genesis of dendritic spines: insights from ultrastructural and imaging studies. *Nat Rev Neurosci*, 5(1):24–34, Jan 2004.

W. Zhang, L. Vazquez, M. Apperson, and M. B. Kennedy. Citron binds to PSD-95 at glutamatergic synapses on inhibitory neurons in the hippocampus. *J Neurosci*, 19(1):96–108, Jan 1999.

J. J. Zhu and R. Malinow. Acute versus chronic NMDA receptor blockade and synaptic AMPA receptor delivery. *Nat Neurosci*, 5(6):513–514, Jun 2002.

J. J. Zhu, Y. Qin, M. Zhao, L. Van Aelst, and R. Malinow. Ras and Rap control AMPA receptor trafficking during synaptic plasticity. *Cell*, 110(4):443–55, Aug 2002.

K. Zito and K. Svoboda. Activity-dependent synaptogenesis in the adult Mammalian cortex. *Neuron*, 35(6):1015–1017, Sep 2002.

Appendices

Appendix A

Expression of synaptic proteins throughout development

In the hippocampus, synapse formation begins during the first week of development. The onset of synapse formation is accompanied by a dramatic increase in the synthesis of synaptic proteins. It is not known however, whether these proteins are co-expressed together or expressed independently. In addition, how these proteins are delivered to synapses, either together as a complex or independently, remains elusive. Determining the exact order and timing of synthesis and delivery of synaptic proteins to synapses would further our understanding of synapse formation.

To approximate the order and timing in expression of various postsynaptic proteins, we determined the relative amounts of PSD-95, the NR2B subunit of the NMDAR and synGAP in mouse hippocampus throughout development (Fig. A.1). We noticed that PSD-95 expression is relatively high at birth and increases gradually thereafter. In the other hand, synGAP expression is very low at birth and dramatically increases in the middle of the first week of development (time at which synapse formation begins) up to adulthood. This resembles the expression of the NR2B subunit of the NMDAR, although the increase is not as steep for NR2B. This suggests that the genes are probably expressed independently of one another. Apparently, PSD-95 precedes synapse formation whereas synGAP is expressed right around the onset of synapse formation. This supports the view that synGAP is crucial for spine

formation, and that changes in protein expression in synGAP *ko* neurons should be studied later in development (Section 6.4).

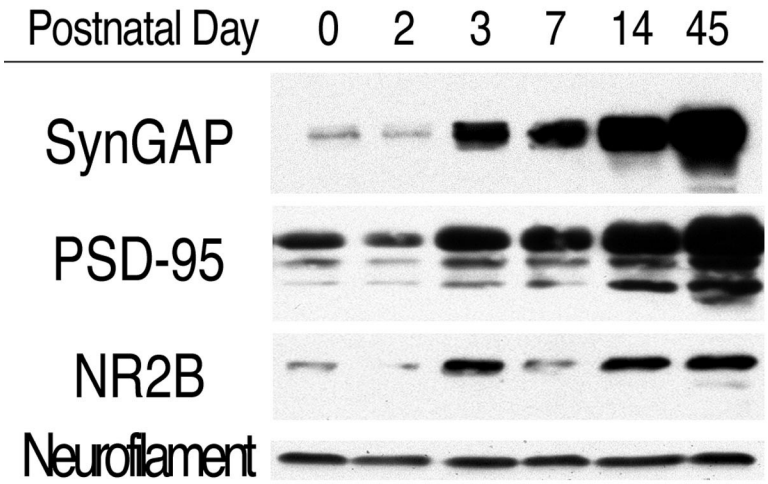

Figure A.1: **Western blot analysis of P1 hippocampal homogenates.** At various developmental stages, mouse hippocampi were homogenized and protein levels were analyzed by Western blot. Synthesis of various synaptic proteins increase gradually increase throughout development.

Appendix B

KS 300 macro for image analysis

```
1  imgdelete "*"
2  Gclear 0
3  # write "@"
4  update
5  MSsetprop "CONDITION","<none>"
6  imagename="    "
7  psdlow=1
8  synlow=1
9  gfplow=1
10 background=1
11 !zviload "D:\Luis\My Documents\120203\nsp gfp\8\8gfp01.zvi",1,"Linear","All",0,1,0,0
12 MSload "puncta"
13 imgstatvalue 1,1,"MAXINDEXY",background
14 write background
15 imgstatvalue 2,1,"MAXINDEXY",background
16 write background
17 normalize 3,900,25
18 highpass 900,904,35,1,2
19 greydilate 904,905,6,6
20 Gextract 905,125,255,12
21 update
22 imgedit 900
23 imgnew 906,1300,1030,1,"Grey"
24 Gmerge 906,255
25 Gclear 0
```

```
binscrap 906,906,0,10000,0
update
binmask 900,906,600
imgedit 600
Gmerge 906,0
Gclear 0
read imagename, "What is the image name?"
imgsave 906, imagename +"-mask.tif"
imgedit 600
imgnew 601,1300,1030,1,"Grey"
Gmerge 601,255
Gclear 0
binand 906,601,603
imgcopy 906,907
imgedit 900
Gmerge 907,255
Gclear 0
update
MSsetprop "REGIONFEAT","AREA","NPARTS"
MSmeasmask 906,3,"mask",1,1,10
binmask 1,907,100
update
imgstatvalue 100,1,"PERC95",synlow
write synlow
high= 250
dislev 100,110,255,255,1
binscrap 110,110,4,300,1
for i54=250; i54 >= synlow; i54 = i54 - 5
        binuerode 110,111,6,0
        dislev 100,120,high,255,1
        binscrap 120,120,4,300,1
        Gextract 111,100,255,12
        Gmerge 120,0
        Gclear 0
        MSsetprop "CONDITION","NPARTS<=1"
        MSlabelmask 120,111,130,1,255
```

```
        binor 110,130,110
        high = high - 5
        # write i45
        # write high
        update
endfor
pause
high= 250
binmask 2,907,200
imgstatvalue 200,1,"PERC95",psdlow
write psdlow
update
dislev 200,210,255,255,1
binscrap 210,210,4,300,1
for i77=250; i77 >= psdlow; i77 = i77 - 5
        binuerode 210,211,6,0
        dislev 200,220,high,255,1
        binscrap 220,220,4,300,1
        Gextract 211,200,255,12
        Gmerge 220,0
        Gclear 0
        MSsetprop "CONDITION","NPARTS<=1"
        MSlabelmask 220,211,230,1,255
        binor 210,230,210
        high = high - 5
        # write high
        update
endfor
pause
high= 250
binmask 3,603,300
imgstatvalue 300,1,"PERC95",gfplow
write gfplow
update
dislev 300,310,255,255,1
binscrap 310,310,1,250,1
```

```
for i99=250; i99 >= gfplow; i99 = i99 - 5
        binuerode 310,311,6,0
        dislev 300,320,high,255,1
        binscrap 320,320,1,250,1
        Gextract 311,200,255,12
        Gmerge 320,0
        Gclear 0
        MSsetprop "CONDITION","NPARTS<=1"
        MSlabelmask 320,311,330,1,255
        binor 310,330,310
        high = high - 5
        # write high
        update
endfor
pause
MSsetprop "CONDITION","<none>"
imgnew 910,1300,1030,1,"Colour"
imgcopy 110,"910[1,1]"
imgcopy 210,"910[1,2]"
imgsave 910,imagename+"-colocalized.tif"
update
dislevrgb 910,911,1,0,100,255,100,255,0,0,11,"RGB"
markobj 110,210,160,1
binxor 110,160,170
markobj 210,110,260,1
binxor 210,260,270
binmask 110,906,116
binmask 160,906,166
binmask 170,906,176
binmask 210,906,216
binmask 260,906,266
binmask 270,906,276
binxor 907,906,908
binmask 110,908,118
binmask 160,908,168
binmask 170,908,178
```

```
binmask 210,908,218
binmask 260,908,268
binmask 270,908,278
MSsetprop "REGIONFEAT","AREA,SUMD,MEAND,MAXD"
MSsetprop "FIELDFEAT","FLDCOUNT[#]=SUM(1),SUMD,FLDMEAND[DENSUNIT]=SUM(SUMD)/SUM(AREA1)"
# MSload "puncta"
MSmeasmask 116,1,"psdtotR",1,1,10
MSmeasmask 166,1,"psdsgoR",1,1,10
MSmeasmask 176,1,"psdsgnR",1,1,10
MSmeasmask 216,2,"sgtotR",1,1,10
MSmeasmask 906,2,"sgR",1,1,10
MSmeasmask 266,2,"sgpsdoR",1,1,10
MSmeasmask 276,2,"sgpsdnR",1,1,10
MSmeasmask 118,1,"pottotR",1,1,10
MSmeasmask 168,1,"potsgoR",1,1,10
MSmeasmask 178,1,"potsgnR",1,1,10
MSmeasmask 908,2,"gotR",1,1,10
MSmeasmask 218,2,"gottotR",1,1,10
MSmeasmask 268,2,"gotpsdoR",1,1,10
MSmeasmask 278,2,"gotpsdnR",1,1,10
wait 200
MSmeasmask 116,1,"psdtotF",1,2,10
MSmeasmask 166,1,"psdsgoF",1,2,10
MSmeasmask 176,1,"psdsgnF",1,2,10
MSmeasmask 906,2,"sgF",1,2,10
MSmeasmask 216,2,"sgtotF",1,2,10
MSmeasmask 266,2,"sgpsdoF",1,2,10
MSmeasmask 276,2,"sgpsdnF",1,2,10
MSmeasmask 118,1,"pottotF",1,2,10
MSmeasmask 168,1,"potsgoF",1,2,10
MSmeasmask 178,1,"potsgnF",1,2,10
MSmeasmask 908,2,"gotF",1,2,10
MSmeasmask 218,2,"gottotF",1,2,10
MSmeasmask 268,2,"gotpsdoF",1,2,10
MSmeasmask 278,2,"gotpsdnF",1,2,10
wait 200
```

```
MSsetprop "REGIONFEAT","SUMD,AREA,OVERLAP[UNIT^2]=SUMD/255,PERCENT[]=(SUMD/255)/AREA*100"
MSmeasmask 166,911,"perpsd",1,1,10
MSmeasmask 266,911,"persg",1,1,10
MSmeasmask 168,911,"perpot",1,1,10
MSmeasmask 268,911,"persgot",1,1,10
beep
stop
```

Appendix C

Abbreviations

AMPAR AMPA-type glutamate receptor

CaMKII Ca^{2+} /calmodulin-dependent protein kinase II

DIV Days *in vitro*

E16 Embryonic day 16

EM Electron microscopy

EPSC excitatory postsynaptic current

ERK 1/2 Extracellularly Regulated Kinase 1 and/or 2

ES Embryonic stem

FIAU Fialuridine

GAP GTP-ase Activating Protein

GAP^{mut} GAP-mutant SynGAP

GEF Guanine nucleotide exchange factor

GFP Green Fluorescent Protein

GluR1 AMPA-type glutamate receptor subunit type 1

het *heterozygote*

ko *knockout*

NGS Normal goat serum

NMDAR NMDA-type glutamate receptor

NR1 NMDA-type glutamate receptor subunit type 1

P1 Post-natal day 1

PBS Phosphate-buffered saline

PH Pleckstrin Homology

PCR Polymerase chain reaction

PSD Post-synaptic density

RasN17 Ras residue 17 point mutant; dominant negative Ras

SEM Standard error of the mean

ΔSXV t-T/SXV motif deleted SynGAP

wt *wild type*

SynGAP^{wt} *wild-type* or full length SynGAP